

Paramagnetic Superconductivity in Extreme Type-II Superconductors

R. R. HAKE

North American Aviation Science Center, Thousand Oaks, California

(Received 19 December 1966)

Magnetization measurements in applied magnetic fields $0 < H \leq 55$ kG and at temperatures $1.2 \leq T \leq 4.2^\circ\text{K}$ have been made on some extremely "dirty" (short electron mean free path) type-II superconducting transition-metal alloys with Gor'kov-Goodman-calculated Ginzburg-Landau κ_G values in the range 30–100: Ti(16 at.% Mo), V(30 at.% Ti) (10 at.% Cr), Ti(22.5 at.% V), and Ti(25 at.% V). Down to the lowest temperatures of measurement, the data show that the high-field superconducting mixed state of such materials is characterized by (a) reversible *paramagnetic* magnetization, (b) second-order transitions at upper critical fields $H_u(T)$ where the paramagnetic superconducting magnetization $M_s(H)$ becomes equal to the paramagnetic normal-state magnetization $M_n(H)$, and (c) parameters $\kappa_1(T) \equiv H_u(T)/[\sqrt{2}H_c(T)]$ (where H_c is the thermodynamic critical field) and $\kappa_2(T) \propto [d(M_s - M_n)/dH]_{H_u}^{-1/2}$ which decrease with decrease of T . The second-order nature of the upper-critical-field transition implies a mixed-state Pauli-paramagnetic conduction-electron spin alignment near $H_u(T)$ which is comparable to that in the high-field normal state. Comparison of the $H_u(T)$, $\kappa_1(T)$, and $\kappa_2(T)$ data with recent extreme type-II theories of Maki and of Werthamer, Helfand, and Hohenberg suggests that electronic spin-flip scattering induced by spin-orbit coupling effectively acts to decouple superconductive spin pairing and thus enhance mixed-state Pauli paramagnetism.

I. INTRODUCTION

MAGNETIZATION measurements have given considerable basic information on type-II superconductors with relatively low Gor'kov-Goodman-calculated Ginzburg-Landau κ_G values.¹⁻⁴ In contrast, the relatively few magnetization studies of "extreme" type-II superconductors ($\kappa_G \gtrsim 20$)⁵⁻⁷ have been somewhat less fruitful because of the gross magnetic irreversibility^{5,6} usually displayed by these materials. This is unfortunate because thermodynamically reversible properties of high- κ_G superconductors, especially those in the very "dirty"⁸ (short electron mean-free-path) domain, are particularly accessible to "clean" theory.⁹⁻¹⁴ Then, too, interesting effects on the mag-

netization of extreme type-II superconductors should be associated with the experimental observation^{15,16} that their resistive upper critical fields¹⁷ H_r are often much lower than the upper critical fields predicted by the original Ginzburg-Landau-Abrikosov-Gor'kov (GLAG) theory,¹⁸⁻²² which ignored electron spin effects. It was previously pointed out^{15,16} that this discrepancy is probably due to preferential Pauli-paramagnetic lowering of normal-state free energy (as originally suggested independently by Clogston²³ and Chandrasekhar²⁴ with respect to the earlier filamentary model), implying the possibility of a first-order transition²³ to the normal state with a *discontinuity* in magnetization. More recent theoretical work²⁵⁻³¹ on electron

¹ E. A. Lynton, *Superconductivity* (Methuen and Company Ltd., London, 1964), 2nd ed.

² See, for example, T. Kinsel, E. A. Lynton, and B. Serin, *Rev. Mod. Phys.* **36**, 105 (1964); W. C. H. Joiner and R. D. Blaugher, *ibid.* **36**, 67 (1964); S. Gyax, *Physik Kondensierten Materie* **4**, 207 (1965); S. T. Sekula and R. H. Kernohan, *J. Appl. Phys.* **36**, 2895 (1965); K. Noto, Y. Muto, and T. Fukuroi, *J. Phys. Soc. Japan* **20**, 467 (1965); T. McConville and B. Serin, *Phys. Rev.* **140**, A1169 (1965); D. K. Finnemore, T. F. Stromberg, and C. A. Swenson, *ibid.* **149**, 231 (1966).

³ G. Bon Mardion, B. B. Goodman, and A. Lacaze, *J. Phys. Chem. Solids* **26**, 1143 (1965).

⁴ R. Radebaugh and P. H. Keesom, *Phys. Rev.* **149**, 217 (1966).

⁵ See, for example, R. M. Bozorth, A. J. Williams, and D. D. Davis, *Phys. Rev. Letters* **5**, 148 (1960); F. J. Morin, J. P. Maita, J. H. Williams, R. C. Sherwood, J. H. Wernick, and J. E. Kunzler, *ibid.* **8**, 275 (1962); J. J. Hauser, *ibid.* **9**, 423 (1962); W. DeSorbo, *Phys. Rev.* **130**, 2177 (1963); W. A. Fietz, M. R. Beasley, J. Silcox, and W. W. Webb, *ibid.* **136**, A335 (1964); L. J. Neuringer and Y. Shapira, *ibid.* **148**, 231 (1966).

⁶ R. D. Blaugher, *Phys. Letters* **14**, 181 (1965).

⁷ P. S. Swartz, *Phys. Rev. Letters* **9**, 448 (1962); G. Meyer, *Phys. Letters* **7**, 93 (1963).

⁸ P. W. Anderson, *J. Phys. Chem. Solids* **11**, 26 (1959). "Dirty" in the Anderson sense means $\xi_0/l > 1$ (see Table II, No. 33).

⁹ K. Maki, *Physics* **1**, 21 (1964).

¹⁰ P. G. de Gennes, *Physik Kondensierten Materie* **3**, 79 (1964).

¹¹ E. Helfand and N. R. Werthamer, *Phys. Rev. Letters* **13**, 686 (1964).

¹² E. Helfand and N. R. Werthamer, *Phys. Rev.* **147**, 288 (1966).

¹³ C. Caroli, M. Cyrot, and P. G. de Gennes, *Solid State Commun.* **4**, 17 (1966).

¹⁴ G. Eilenberger, *Phys. Rev.* **153**, 584 (1967).

¹⁵ T. G. Berlincourt and R. R. Hake, *Phys. Rev. Letters* **9**, 293 (1962).

¹⁶ T. G. Berlincourt and R. R. Hake, *Phys. Rev.* **131**, 140 (1963).

¹⁷ We designate *measured* upper critical fields as H_r (resistive) and H_u (magnetization or specific heat), *theoretical* upper critical fields as H_{c2}^* (neo-GLAG theory without Pauli spin effects) and H_{c2} (theory including Pauli spin effects), and use subscript "0" to indicate $T = 0^\circ\text{K}$.

¹⁸ V. L. Ginzburg and L. D. Landau, *Zh. Eksperim. i Teor. Fiz.* **20**, 1064 (1950); V. L. Ginzburg, *Nuovo Cimento* **2**, 1234 (1955).

¹⁹ A. A. Abrikosov, *Zh. Eksperim. i Teor. Fiz.* **32**, 1442 (1957) [English transl.: *Soviet Phys.—JETP* **5**, 1174 (1957)].

²⁰ L. P. Gor'kov, *Zh. Eksperim. i Teor. Fiz.* **36**, 1918 (1959) [English transl.: *Soviet Phys.—JETP* **9**, 1364 (1959)].

²¹ L. P. Gor'kov, *Zh. Eksperim. i Teor. Fiz.* **37**, 835 (1959) [English transl.: *Soviet Phys.—JETP* **10**, 593 (1960)].

²² L. P. Gor'kov, *Zh. Eksperim. i Teor. Fiz.* **37**, 1407 (1959) [English transl.: *Soviet Phys.—JETP* **10**, 998 (1960)].

²³ A. M. Clogston, *Phys. Rev. Letters* **9**, 266 (1962).

²⁴ B. S. Chandrasekhar, *Appl. Phys. Letters* **1**, 7 (1962).

²⁵ K. Maki and T. Tsuneto, *Progr. Theoret. Phys. (Kyoto)* **31**, 945 (1964).

²⁶ G. Sarma and D. Saint-James, in *Proceedings of the Conference on the Physics of Type-II Superconductivity, 1964* (to be published).

²⁷ K. Maki, *Physics* **1**, 127 (1964).

²⁸ K. Maki, *Phys. Rev.* **148**, 362 (1966).

²⁹ N. R. Werthamer, E. Helfand, and P. C. Hohenberg, *Phys. Rev.* **147**, 295 (1966).

³⁰ D. Saint-James, *Phys. Letters* **23**, 177 (1966).

³¹ D. Saint-James, G. Sarma, and E. J. Thomas (to be published).

spin effects within the type-II framework and more recent experimental H_c ³²⁻³⁹ and flux-flow^{32,33,39,40} measurements have generally tended to confirm the early suggestions^{15,16,23,24} of a paramagnetic limitation on superconductors with very high upper critical fields.

Recently we succeeded in fabricating some extreme type-II superconducting specimens which displayed *reversible* high-field magnetization behavior.⁴¹ Resistive and ballistic magnetization measurements in applied magnetic fields $0 < H \leq 27$ kG showed that these materials were characterized by a new type of reversible *paramagnetic* superconductivity in the high-field mixed state with *no apparent discontinuity* in magnetization at the upper critical field¹⁷ $H_u(T)$, where the paramagnetic superconducting magnetization $M_s(H)$ became equal to the paramagnetic normal-state magnetization $M_n(H)$. Cape,⁴² utilizing a sensitive vibrating-sample magnetometer at $0 < H \leq 50$ kG, corroborated⁴³ this result for one of these alloys, Ti(16 at. % Mo),⁴⁴ and showed that the parameter

$$\kappa_2(T) \propto [d(M_s - M_n)/dH]_{H_u}^{-1/2}$$

decreased with decrease of T , in contrast to the behavior of low- κ_G type-II superconductors.^{2-4,13,14} He compared his $H_u(T)$ and $\kappa_2(T)$ data for Ti(16 at. % Mo) with recent and independent extreme type-II spin-effect theories of Maki²⁸ and of Werthamer, Helfand, and Hohenberg (WHH),²⁹ and thereby adduced evidence for the influence of spin-orbit-coupling induced electronic spin-flip scattering. Maki and Tsuneto²⁵ had earlier suggested a possible enhancement of upper

critical fields by spin-orbit interaction, after showing that¹⁷ H_{c2} as predicted by a Gor'kov-equation²⁰⁻²² analysis which included Pauli spin terms fell below the measured^{15,16} H_c values for Ti-V alloys.

More recently, calorimetric measurements by Barnes and Hake⁴⁵ on Ti(16 at. % Mo) at $0 \leq H \leq 29$ kG convincingly demonstrated the existence of sharp bulk-material second-order transitions from the paramagnetic superconducting mixed state to the paramagnetic normal state at fields reasonably close to the magnetization indicated $H_u(T)$ values. These measurements also yielded values for the transition specific-heat jump $\Delta C(H_u, T_s) \propto \kappa_2^{-2}(dH_u/dT)^2 T_s$ and the thermodynamic critical field $H_c(T)$, and thereby showed directly that *both* $\kappa_2(T)$ and

$$\kappa_1(T) \equiv H_u(T)/[\sqrt{2}H_c(T)]$$

decreased with decrease of T .

In the present paper⁴⁶ we report ballistic magnetization measurements at $0 < H \leq 55$ kG and at temperatures $1.2 \leq T \leq 4.2^\circ\text{K}$ on some of the extreme type-II superconductors previously measured⁴¹ at lower H : Ti(16 at. % Mo), V(30 at. % Ti)(10 at. % Cr), Ti(22.5 at. % V), and Ti(25 at. % V).^{47,48} The initial flux-penetration fields, the shapes of paramagnetic superconducting magnetization curves, magnetization peak effects, mixed- and normal-state free energies, and the (H - T) phase diagram characteristic of the present high- κ_G superconductors are discussed. Resistive and sheath behavior are only briefly mentioned, since this aspect will be the subject of a succeeding paper.⁴⁹ The qualitative significance of paramagnetic mixed-state magnetization is then considered with reference to the effect of superconductive Cooper spin pairing on the behavior of $H_u(T)$, $\kappa_1(T)$, and $\kappa_2(T)$. Finally, the experimental data are compared with the predictions of Maki²⁸ and WHH,²⁹ after review of the salient results and limits of applicability of those theories.

II. SPECIMENS

Table I lists some electronic parameters and critical fields of the six polycrystalline, bcc, solid-solution alloy specimens examined in the present study. All the specimens are characterized by (1) a high Gor'kov-Goodman-calculated Ginzburg-Landau parameter κ_G , (2) a high normal-state electrical resistivity ρ_n (4.2°K),

³² Y. B. Kim, C. F. Hempstead, and A. R. Strnad, Phys. Rev. **139**, A1163 (1965). Flux-flow measurements reported in this reference (and in later work of Refs. 33, 39, and 40) apparently show that for the low- t , high- κ_G case the mixed-state vortex-core-to-specimen-volume ratio is proportional to H/H_{c20}^* rather than H/H_{c0} where $H_{c0} \ll H_{c20}^*$ is the observed resistive upper critical field.

³³ Y. Shapira and L. J. Neuringer, Phys. Rev. **140**, A1638 (1965).

³⁴ Y. B. Kim and A. R. Strnad, in *Quantum Fluids*, edited by D. F. Brewer (North-Holland Publishing Company, Amsterdam, 1966), p. 68.

³⁵ K. M. Ralls, R. M. Rose, and J. Wulff, J. Appl. Phys. **36**, 1295 (1965); D. A. Colling, K. M. Ralls, and J. Wulff, Trans. AIME **236**, 1218 (1966).

³⁶ D. B. Montgomery and H. Witzgall, Phys. Letters **22**, 48 (1966). A WHH fit to these data yield $\lambda_{90}(t=0.2) \approx 0.25$ for $V_3\text{Ga}$ and $V_{4.6}\text{Ga}$, but larger λ_{90} values are required to fit the higher t data. Judging by the high measured resistivity $\rho_n = 0.41 \times 10^{-4} \Omega \text{ cm}$, the $V_3\text{Ga}$ specimen is probably "dirty."

³⁷ L. J. Neuringer and Y. Shapira, Phys. Rev. Letters **17**, 81 (1966).

³⁸ S. J. Williamson, in Proceedings of the Tenth International Conference on Low-Temperature Physics, 1966 (to be published).

³⁹ Y. B. Kim, in Proceedings of the Tenth International Conference on Low-Temperature Physics, 1966 (to be published).

⁴⁰ R. R. Hake, Bull. Am. Phys. Soc. **11**, 480 (1966).

⁴¹ R. R. Hake, Phys. Rev. Letters **15**, 865 (1965).

⁴² J. A. Cape, Phys. Rev. **148**, 257 (1966).

⁴³ Paramagnetic mixed-state magnetization over a wide field range has also recently been observed for a Ti(50 at. % V) alloy by Y. Shibuya and T. Aomine, in Proceedings of the Tenth International Conference on Low-Temperature Physics, 1966 (to be published).

⁴⁴ The designation A (N at. % B) indicates a solid solution of N atomic percent of metal B in metal A .

⁴⁵ L. J. Barnes and R. R. Hake, Bull. Am. Phys. Soc. **11**, 709 (1966); Phys. Rev. **153**, 435 (1967); Ann. Acad. Sci. Fennicae, Ser. A, **VI**, 78 (1966).

⁴⁶ A preliminary report of this work has been given by R. R. Hake, Bull. Am. Phys. Soc. **10**, 1207 (1965). The relevance of the present considerations to upper-critical-field limits for bulk type-II superconductors has been discussed by R. R. Hake, Appl. Phys. Letters **10**, 189 (1967).

⁴⁷ Resistive and flux-flow measurements on these alloys have been reported (Ref. 40).

⁴⁸ For a brief report on magnetization and resistive behavior of these alloys, see R. R. Hake, in Proceedings of the Tenth International Conference on Low-Temperature Physics, 1966 (to be published).

⁴⁹ R. R. Hake (to be published).

TABLE I. Some electronic parameters and critical fields for the six extreme type-II superconducting alloys of the present study.

Alloy	κ_G^a	T_c^b (°K)	$\rho(4.2^\circ\text{K})^c$ ($\mu\Omega\text{cm}$)	α^d	α^2	$H_{fp}(4.2^\circ\text{K})^e$ (kG)	$H_{ps}(4.2^\circ\text{K})^f$ (kG)	$H_u(4.2^\circ\text{K})^g$ (kG)	Condition ^h
Ti(16 at.% Mo) No. 1 ⁱ	68	4.18 ^j	103	1.81	3.28	0.048(3°K)	13.5(3°K)	34.5(3°K)	an
V(30 at.% Ti) (10 at.% Cr) No. 1 ⁱ	35	5.6 ^k	45	1.16	1.34	0.144	15	29	an
Ti(22.5 at.% V) No. 2	100	4.7 ^k	146	2.81	7.90	0.017	5.2	24	ac
Ti(25 at.% V) No. 1 ⁱ	99	5.3 ^k	135	2.95	8.70	0.042	16	...	ac
Ti(25 at.% V) No. 2 ⁱ	97	5.3 ^k	132	2.88	8.32	...	17	≈52	cr
Ti(25 at.% V) No. 3	95	5.6 ^k	129	2.82	7.95	0.067	32	>53	an

^a Ginzburg-Landau parameter calculated from the Gor'kov-Goodman formula, Eq. (A13c).

^b Superconducting transition temperature.

^c Normal-state electrical resistivity.

^d Maki paramagnetic limitation parameter calculated from Eq. (A18b).

^e Initial flux-penetration field.

^f Field at onset of paramagnetic superconductivity.

^g Magnetization-determined upper critical field.

^h ac: specimen machined from material which had been arc cast on a water-cooled copper hearth; specimen not annealed. cr: specimen machined from material which had been cold rolled to a thickness reduction of about 2:1; specimen not annealed. an: specimen annealed (after machining) for 1 h at

0.8 of the melting point in a vacuum of about 3×10^{-6} mm Hg with a cooling rate (for metastable Ti-Mo and Ti-V) after annealing of $\approx 7^\circ\text{C}/\text{min}$ to 800°C , $\approx 70^\circ\text{C}/\text{min}$ to 500°C , $\approx 30^\circ\text{C}/\text{min}$ to 350°C , $15^\circ\text{C}/\text{min}$ to 20°C ; except for V (30 at.% Ti) (10 at.% Cr) all annealed specimens had been cold-rolled to a thickness reduction of about 2:1 prior to machining and annealing. All specimens were subjected to a slow chemical etch (polish) prior to measurement so as to reduce possible compositional and defect nonuniformity near the specimen surface.

ⁱ Same specimen as in Ref. 1.

^j From extrapolation of $H_u(T)$ to $H_u(T_c)=0$.

^k From resistive-onset measurements at $0.3 \leq J \leq 3$ A/cm².

(3) a high Maki²⁸ paramagnetic limitation parameter α , (4) a relatively low superconducting transition temperature T_c , and (5) a relatively good alloy homogeneity with low precipitate concentration [except for Ti(25 at.% V) No. 3]. Table II presents a more complete list of relevant electronic properties for four of these very dirty type-II superconductors, either measured or calculated (in some cases estimated) using Eqs. (A1)–(A19) of the Appendix.

Figure 1(a–c) shows photomicrographs of samples having composition, fabrication, and heat-treatment histories identical to those of the measured specimens Ti(16 at.% Mo) No. 1, Ti(25 at.% V) No. 1, and Ti(25 at.% V) No. 3. The annealed Ti(16 at.% Mo) alloy appears to be virtually free of “coring,” segregation, and impurity precipitates. This apparent metallurgical homogeneity and purity correlate with good reversibility of the high-field magnetization (Figs. 3 and 4). The sample representative of Ti(25 at.% V) No. 1 displays a relatively low degree of dendritic coring for an as-arc-cast alloy, apparently because of the near congruence of the solidus and liquidus curves at this composition.⁵⁰ Here, again, homogeneity and purity correlate with high-field magnetization reversibility [Fig. 10(a)]. The photomicrograph representative of Ti(25 at.% V) No. 3 shows an unidentified annealing-induced precipitate which produces markedly irreversible high-field magnetization behavior [Fig. 10(c)].

Except for V(30 at.% Ti) (10 at.% Cr), all the specimens of Table I belong to a class of metastable bcc group-IV-rich alloys which display very high

normal-state electrical resistivities.⁵¹ At sufficiently low addition-element concentrations, the resistivities are also markedly anomalous in their dependence on temperature and solute concentration.⁵¹ The electronic, superconducting, and metallurgical characteristics of such alloys, as well as the arc-melting procedures for their preparation, have been previously discussed.^{51–53} All the specimens were machined to cylindrical form with hemispherical ends and with length ≈ 21 mm, diam ≈ 1.5 mm, and demagnetizing coefficient¹ $D \approx 0.010$. The metallurgical condition of each as-measured specimen is indicated in Table I.

III. APPARATUS AND METHOD

A. Magnetic Fields

The magnetization measurements were made in applied magnetic fields up to 55 kG generated by a

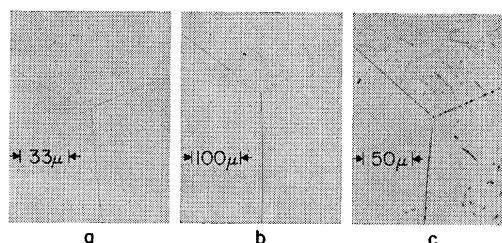


Fig. 1. Photomicrographs representative of (a) Ti(16 at.% Mo) No. 1 (annealed), (b) Ti(25 at.% V) No. 1 (as arc cast), and (c) Ti(25 at.% V) No. 3 (annealed), as discussed in the text and indicated in Table I.

⁵¹ R. R. Hake, D. H. Leslie, and T. G. Berlincourt, J. Phys. Chem. Solids **20**, 177 (1961).

⁵² R. R. Hake, Phys. Rev. **123**, 1986 (1961).

⁵³ R. R. Hake and D. H. Leslie, J. Appl. Phys. **34**, 270 (1962).

⁵⁰ M. Hansen, *Constitution of Binary Alloys* (McGraw-Hill Book Company, Inc., New York, 1958), p. 1241.

TABLE II. Electronic properties of four extreme type-II superconducting alloys.

Property	N ^a or S	M ^b or equation indicated	Ti(16 at. % Mo) No. 1	V(30 at. % Ti) (10 at. % Cr) No. 1	Ti(22.5 at. % V) No. 2	Ti(25 at. % V) No. 2	Units
1. Electrical resistivity ρ_0 (4.2°K)	N	M	1.03 ^e	0.45 ^e	1.46 ^e	1.32 ^e	10 ⁻⁴ Ω cm
2. Electronic-specific-heat coefficient γ	N	M	0.749 ^d	≈1.10 ^e	0.82 ^f	0.93 ^f	10 ⁴ erg/cm ³ (°K) ²
3. Density of states N (one spin direction)	N	(A5)	1.62	≈2.00	2.12	1.95	ev ⁻¹ atom ⁻¹
4. Magnetic susceptibility χ_0 (4.2°K)	N	M	1.8 ^e	3.0 ^e	1.9 ^e	2.0 ^e	10 ⁻⁶ emu cm ⁻³
5. Pauli spin susceptibility $\chi_P(N)$	N	(A6)	1.03	1.51	1.12	1.27	10 ⁻⁶ emu cm ⁻³
6. Atomic volume V_a (4.2°K)	N	≈M	10.2 ^e	8.58 ^e	9.97 ^e	9.91 ^e	cm ³ mole ⁻¹
7a. Conduction electrons n_c per atom ^h	N	...	4.32	4.80	4.23	4.25	atom ⁻¹
b. Conduction electrons n per cm ³ ^h	N	...	2.55	3.37	2.55	2.58	10 ²³ cm ⁻³
8. Average atomic number \bar{Z}	N	...	25.2	22.8	22.2	22.2	...
9. $\langle 1/V_F \rangle^{-1} \leq \langle V_F \rangle \equiv$ average Fermi velocity	N	(A1) ⁱ	1.9 ⁱ	1.5 ^j	1.7 ⁱ	1.5 ^j	10 ⁷ cm sec ⁻¹
10. Electronic mean free path l	N	(A2) ⁱ	5.1 ^j	9.7 ^j	3.6 ^j	4.0 ^j	Å
11. Thermal effective-mass ratio (m^*/m) _t	N	(A3)	7.28	9.74	7.97	9.00	...
12a. Transport scattering time $\tau_{tr} \approx l \langle 1/V_F \rangle$	N	(A4) ⁱ	2.8 ^j	6.4 ^j	2.1 ^j	2.6 ^j	10 ⁻¹⁶ sec
b. Transport scattering frequency τ_{tr}^{-1}	N	(A4) ⁱ	3.6 ^j	1.6 ^j	4.7 ^j	3.8 ^j	10 ¹⁴ sec ⁻¹
13. Superconducting transition temperature T_c	S	M	4.18 ^{e,k}	5.6 ^{e,l}	4.7 ^{e,l}	5.3 ^{e,l}	°K
14a. Thermodynamic critical field H_{c0} at 0°K from $C(T)$	S	M ^p	0.890 ^d	kG
b. Thermodynamic critical field H_{c0} at 0°K from $M(H)$	S	M ^q	<0.985 ^e	...	<1.10 ^e	<1.94 ^e	kG
c. Thermodynamic critical field H_{c0} at 0°K (BCS)	S	(A12b)	0.875	1.36	1.03	1.24	kG
d. Thermodynamic critical field $H_c(4.2°K)$ at 4.2°K (BCS)	S	(A12a)	...	0.55	0.187	0.42	kG
15a. Intrinsic Ginzburg-Landau parameter κ_0	S	(A13a) ⁱ	0.8	1.2	1.0	1.3	...
b. Extrinsic Ginzburg-Landau parameter κ_l	S	(A13b)	66.8	33.9	99.1	95.5	...
c. Total Ginzburg-Landau parameter κ_G	S	(A13c) ⁱ	67.6	35.1	100.0	96.8	...
16. $\kappa_1(T_c) \equiv \text{Lim}_{T \rightarrow T_c} [H_u(T)/\sqrt{2}H_c(T)]$	S	(A14)	69.3
17. Upper critical field at 0°K H_{u0}	S	≈M	63.0	...	≈81.0 ^m	≈90.0 ^m	kG
18a. $(dH_u/dT)_{T_c}$	S	M	-36.0 ^e	kG(°K) ⁻¹
b. $(dH_u/dT)_{T_c}$	S	(A18c)	...	-22.0	-53.0	-54.0	kG(°K) ⁻¹
19a. Lower critical field at 0°K H_{c10}	S	M ^o	<0.075 ^e	kG
b. Lower critical field at 0°K H_{c10}	S	{(A12a, b) (A13c) (A15)}	0.028	0.071	0.024	0.029	kG
c. Lower critical field $H_{c1}(4.2°K)$	S	0.037	0.006	0.013	kG
d. Lower critical field $H_{c1}(4.2°K)$	S	M ^o	...	<0.144 ^e	<0.017 ^e	...	kG

Table II (Continued)

Property	N ^a or S	M ^b or equation indicated	Ti (16 at.-% Mo) No. 1	V (30 at.-% Cr) No. 1	Ti (22.5 at.-% V) No. 2	Ti (25 at.-% V) No. 2	Units
20a. Neo-GLAG upper critical field H_{c0}^* at 0°K	S	(A16b)	98.7	84.4	172.	199.0	kG
b. Neo-GLAG upper critical field H_{c0}^* at 0°K	S	(A16c)	104.0	kG
c. H_{c0}^* from flux-flow	S	M	111.0 ^m	...	≈209.0 ⁿ	...	kG
21. Clogston upper-critical-field limit H_{F0}	S	(A17b)	76.9	103.0	86.5	97.5	kG
22a. Maki paramagnetic limitation parameter α	S	(A18b)	1.81	1.16	2.81	2.88	...
b. Maki paramagnetic limitation parameter α	S	(A18c)	1.91
c. α^2	S	(A18b)	3.28	1.35	7.92	8.32	...
23. BCS coherence length ξ_0	S	(A7) ⁱ	611.0 ⁱ	374.0 ⁱ	496.0 ⁱ	391.0 ⁱ	Å
24. Ginzburg-Landau coherence length ξ_0 at 0°K	S	(A8)	≈56.0	≈60.0	≈42.0	≈39.0	Å
25. Electromagnetic coherence length ξ_0	S	(A9) ⁱ	5.1 ⁱ	9.5 ⁱ	3.6 ⁱ	3.9 ⁱ	Å
26. London penetration depth λ_{L0} at 0°K	S	(A10) ⁱ	477.0 ⁱ	460.0 ⁱ	499.0 ⁱ	527.0 ⁱ	Å
27. Penetration depth λ_0 at 0°K	S	(A11)	5210.0 ⁱ	2980.0 ⁱ	5850.0 ⁱ	5300.0 ⁱ	Å
28. $\beta_0^2 \equiv e^2 / (1.78\lambda_{00})$, from κ_2^*	S	≈M	2.0 ^e	≈0.9 ^e	≈3.3 ^e	≈4.0 ^e	...
29a. Spin-flip frequency parameter λ_{90} from κ_2^*	S	≈M	0.9 ^e	≈0.8 ^e	≈1.3 ^e	≈1.2 ^e	...
b. Spin-flip frequency parameter λ_{90} from h^*	S	≈M	0.5 ^e	≈1.0 ^e	≈0.6 ^e
30a. Spin-flip scattering time τ_{90} from κ_2^*	S	(A19)	2.2	1.8	1.3	1.3	10 ⁻¹³ sec
b. Spin-flip scattering time τ_{90} from h^*	S	(A19)	3.9	1.4	2.9	...	10 ⁻¹³ sec
c. Spin-flip scattering frequency τ_{90}^{-1} from κ_2^*	S	(A19)	4.5	5.6	7.7	7.7	10 ¹² sec ⁻¹
d. Spin-flip scattering frequency τ_{90}^{-1} from h^*	S	(A19)	2.6	7.1	3.4	...	10 ¹² sec ⁻¹
31a. τ_{90} / τ_{90} (from κ_2^*)	S	(A4) ⁱ , (A19)	0.013 ⁱ	0.035 ⁱ	0.016 ⁱ	0.020 ⁱ	...
b. τ_{90} / τ_{90} (from h^*)	S	(A4) ⁱ , (A19)	0.007 ⁱ	0.044 ⁱ	0.007 ⁱ
32. $l_{90} \approx \langle V_F \rangle \tau_{90}$, spin-flip mean free path (τ_{90} from h^*)	S	(A1) ⁱ , (A19)	737.0 ⁱ	217.0 ⁱ	490.0 ⁱ	...	Å
33. ξ_0 / l	S	(A2) ⁱ , (A7) ⁱ	120.0 ⁱ	38.0 ⁱ	138.0 ⁱ	99.0 ⁱ	...
34. $\kappa_2^* (t_0) / \kappa_1^* (t_0)$ (t_0 = lowest measurement $l \equiv l / T_0$)	S	M	0.78 ($t_0 = 0.37$)	0.82 ($t_0 = 0.48$)	0.87 ($t_0 = 0.73$)	0.70 ($t_0 = 0.79$)	...

^a Normal-state N or superconducting-state S property.
^b Measured M or from equation indicated.
^c From present measurements.
^d From specific-heat measurements of Ref. 45, after applying -0.4 and -1.7% corrections to the calorimetrically measured γ and H_{c0} , respectively, so as to make approximate allowance for the -1.6% difference in the measured transition temperatures of calorimetric ($T_c = 4.246^\circ\text{K}$) and magnetization ($T_c = 4.18^\circ\text{K}$) specimens. It is assumed from BCS (Ref. 96) that $dH_{c0}/H_{c0} = 0.5 \delta\gamma/\gamma + dT_c/T_c$ and $\delta\gamma/\gamma \approx [\ln(0.85 \Theta_D/T_c)]^{-1} dT_c/T_c = 0.25 dT_c/T_c$.
^e Estimate.
^f From specific-heat measurements of Ref. 101.
^g Derived from data in W. B. Pearson, *Handbook of Lattice Spacings and Structures of Metals and Alloys* (Pergamon Press, Inc., New York, 1958), pp. 567, 763, 876. A 1% volume contraction between room temperature and 4.2°K has been assumed.
^h Assumed equal to the average number of electrons outside closed shells.
ⁱ The usual assumption is made that $S/S_0 = 0.6$ (see Refs. 16, 98, and 99).
^j Rough approximation.
^k From extrapolation of $H_{c0}(T)$ to $H_{c0}(T_c) = 0$.
^l From resistive-onset measurements at $0.3 \leq J \leq 3$ A/cm².
^m From Ref. 16.
ⁿ From Refs. 48, 49.
^o The initial-flux-penetration field $H_{F0}(T)$ or $H_{F0}(T \rightarrow 0)$ is given as the upper limit to $H_{c1}(T)$ or $H_{c1}(T = 0)$.
^p By double integration of the measured zero-field $C_n(T)/T$ and $C_s(T)/T$.
^q From area enclosed by $M_n(H)$ and $M_s(H)$. The extrapolation to $T = 0$ assumes that H_c is a linear function of T .

nested pair of superconducting solenoids, perfect-layer wound in our laboratory using a total of 44 000 ft (55 000 turns) of Nb(25 at.% Zr) wire,⁵⁴ a winding tension of 4 lb, and an 0.002-in.-thick Mylar sheet between layers. The outer copper-form solenoid was the same high-homogeneity 3-in.-i.d., 5.5-in.-o.d., 6-in.-long Helmholtz-pair⁵⁵ magnet used at $H \leq 29$ kG for the earlier magnetization⁴¹ and specific-heat⁴⁵ studies. The inner beryllium-copper-form solenoid had a 1-in. i.d., a 2.8-in. o.d., and a 8-in. length, sufficient for an axial-field homogeneity⁵⁶ matching that of the outer solenoid. The two solenoids were series connected, shunted by a 10- Ω resistor outside the helium bath, and energized by a transistorized dc power supply with a gear-driven current control. Despite the considerable stored energy (magnet inductance ≈ 40 H), complete recovery of the magnet was always observed after quenching at 16–18 A. The magnet was calibrated using a nominally 0.1% accurate Rawson null-deflection cryogenic rotating-coil gaussmeter. Axial-field measurements at 3.5 and 32 kG indicated field homogeneities of ± 0.05 and $\pm 0.1\%$ over axial distances of 3.0 and 3.6 cm, respectively. The magnet “constant” $C \equiv H/I$ (where H is the central average field for 0.1% homogeneity and I is the magnet current) was measured as $C = 3.4010, 3.3815$ kG/A at $H = 3.5, 32$ kG, respectively.⁵⁷ In the present work, H was determined from the measured magnet current, assuming $C = 3.39$ kG/A independent of I , and the earth’s field was not compensated.

B. Magnetization Measurement

The isothermal magnetization measurements were made in a standard ballistic manner.⁵⁸ The 2.1-cm-long specimen was moved smoothly a distance 2.2 cm within the effectively time-independent, spatially homogeneous ($\pm 0.15\%$) H from the center of one 18 000-turn search coil (2.1-mm i.d., 11-mm o.d., 9.5-mm length) to the center of another identical but oppositely wound search coil. (The search coils sampled only the central portion of the specimen so as to avoid possible end-effect complications.) The deflection of a nearly zero-restoring-torque fluxmeter⁵⁹ connected in series with the search coils was then just propor-

tional to the specimen magnetization $M(H)$. A proportionality constant was determined for each specimen by measurement of its magnetization in the “perfectly” diamagnetic low- H Meissner state [where $M(H) = -H/4\pi$ (see Fig. 2), to within $\approx 1\%$ for the present low-demagnetizing-coefficient specimens]. The double-search-coil bobbin was made of beryllium-copper, had a wall thickness of ≈ 0.25 mm, and was wound with No. 46 heavy-Formex-insulated copper wire of total resistance $\approx 140 \Omega$ at 4.2°K. Sensitivity of the magnetometer was such that an ≈ 7.0 -mm deflection was obtained upon movement of the present specimens in the “perfectly” diamagnetic Meissner state with $H = 10$ G. Fluxmeter deflections could generally be read and reproduced to ± 0.1 mm for deflections less than 50 mm, amounting to an uncertainty in $4\pi M$ of $\pm 1.4\%$ at $4\pi M = 10$ G. An added uncertainty of $\approx \pm 10\%$ in $4\pi M$ results from (a) an $\approx 5\%$ uncertainty in the magnet “constant” C ($H \lesssim 50$ G) in the low-field Meissner-state region where the magnetization-deflection relationship was determined, and (b) possible perturbation of the magnetometer signal in high fields by paramagnetic solid-air impurities in the liquid helium surrounding the specimen.⁶⁰ The general reliability and accuracy of the magnetometer was confirmed by $M(H)$ measurements on (1) various standard type-I and type-II superconductors, (2) normal metals and alloys, both diamagnetic and paramagnetic, and with and without localized moments, and (3) the empty 0.25-mm-wall beryllium-copper specimen holder. A 0.2-mm paramagnetic deflection was observed for the empty holder at 50 kG, about 1–3% of that observed during actual measurement of the present specimens at that field.

C. Cryogenics

The magnet, specimen, and magnetometer coils were rigidly suspended in liquid helium contained in a 6-in.-i.d., 46-in.-deep double-wall Pyrex-glass Dewar. Temperatures down to 1.18°K were obtained by pumping over the helium bath with a 500-ft³/min mechanical pump connected to the Dewar through a 6-in. copper line with vibration-damping concrete-block and metal-bellows inserts. Temperatures were held constant to within 0.005 K° and were determined to about $\pm 1\%$ by measurement of the helium vapor pressure (T58 scale⁶¹) over the helium bath with mercury and oil manometers read with a Wild Heerbrugg cathetometer. Hydrostatic head corrections were not made.

⁵⁴ From Supercon division of the National Research Corporation; type “A25” wire: 0.010-in. diam with 0.001-in.-thick Formex insulation over 0.001-in.-thick copper plating.

⁵⁵ The central gap spacing was ≈ 0.25 in., in accord with the calculations of M. W. Garrett as given by D. B. Montgomery and J. Terrell, National Magnet Laboratory Report No. AFOSR-1525, 1961 (unpublished), Tables 3–5.

⁵⁶ D. E. Mapother and J. N. Snyder, University of Illinois Engineering Experiment Station Circular No. 66, 1955 (unpublished).

⁵⁷ Similar H dependence of $C \equiv H/I$ for a superconducting magnet has been observed by B. W. Maxfield and J. R. Merrill, Rev. Sci. Instr. **36**, 1083 (1965).

⁵⁸ D. Shoenberg, *Superconductivity* (Cambridge University Press, New York, 1952), 2nd ed., p. 53; W. E. Henry, Phys. Rev. **88**, 559 (1952).

⁵⁹ General Electric Model 9892910-G154.

⁶⁰ Spurious signals were sometimes observed after accidental air leaks into the liquid helium. This solid air impurity problem has recently been discussed by W. F. Giauque, R. A. Fisher, E. W. Hornung, R. A. Butera, and G. E. Brodale, J. Chem. Phys. **42**, 9 (1965).

⁶¹ H. van Dijk, M. Durieux, J. R. Clement, and J. K. Logan, J. Res. Natl. Bur. Std. **A64**, 4 (1960).

D. Resistive Measurements

Electrical resistance measurements^{47,48} in longitudinal H were made in a standard four-lead manner^{62,63} using the same specimens, magnet, and Dewar system as for the magnetization measurements. Nondestructive copper current-lead and potential-lead contacts were pressed firmly against the specimens by beryllium-copper-strip springs. The potential-lead contacts were spaced 9.5 mm apart along the longitudinal axis of the specimen so as to sample the same central portion of the specimen sensed by the search coils in the magnetization measurement. Absolute values of the resistivity listed in Table I may be in error by $\pm 3\%$ owing primarily to uncertainty in specimen dimensions and in potential-lead separation.

Zero-field transition temperatures above 4.2°K, listed in Table I, were measured resistively, utilizing a probe similar to that described above, except that an 8-in.-long stainless-steel-tube lower extension was clamped to the cylindrical Micarta specimen mount. The specimen was tightly wrapped with cotton⁶⁴ and aluminum foil and the depth of immersion of the tube extension and the attached copper current and potential leads was adjusted to obtain a slow warmup of the specimen above 4.2°K. Temperatures were measured with a Cu-to-Au (0.07 at. % Fe)⁶⁵ thermocouple.⁶⁶ The primary junction was pressed against the specimen, and the reference junction was placed at the end of the extension so as to remain in the liquid-helium bath at 4.2°K. The thermocouple was calibrated via the superconducting transition temperature of pure Pb⁶⁷ [$\rho(295^\circ\text{K})/\rho_n(4.2^\circ\text{K}) \equiv RR = 10^4$, $T_c = 7.19^\circ\text{K}$], pure Bureau of Mines V⁶⁸ ($RR = 153$, $T_c = 5.38^\circ\text{K}$), and pure Ta⁶⁹ ($RR = 46$, $T_c = 4.43^\circ\text{K}$). Thermocouple sensitivity appeared to be nearly constant at $12 \mu\text{V}/\text{K}^\circ$ at $4.2 < T < 7.2^\circ\text{K}$. The resistance-versus-temperature transitions were observed on an X-Y recorder and T_c was taken as the temperature at which a sharp resistive onset occurred. These onsets were found to be reproducible to about $\pm 0.05^\circ\text{K}$ and to be independent of measuring current density J for $0.3 \leq J \leq 3 \text{ A}/\text{cm}^2$. T_c values so obtained are probably accurate to $\pm 0.1^\circ\text{K}$.

IV. EXPERIMENTAL RESULTS

A. Ti(16 at. % Mo)

Figures 2-4 show isothermal magnetization curves for the annealed specimen Ti(16 at. % Mo) No. 1. As H is increased from zero at constant $T < T_c$, a superconducting magnetization $M_s(H)$ is initially observed which is qualitatively similar to that of quasireversible low- κ_G type-II materials¹⁻⁴; nearly perfect flux exclusion (diamagnetism) up to an initial flux penetration field $H_{fp}(T)$, as shown in Fig. 2, followed by gradual mixed-state flux penetration with consequent gradual approach of $M_s(H)$ to zero as shown in Figs. 3 and 4. With further increase of H , $M_s(H)$ crosses the zero- M axis at a paramagnetic-superconductivity onset field $H_{ps}(T)$, and becomes increasingly paramagnetic. The $M_s(H)$ curve finally contacts the normal-state paramagnetic magnetization line $M_n(H)$ at a magnetization-determined upper critical field $H_u(T)$. On the return decreasing- H cycle, the magnetization is observed to be reversible at high fields and irreversible at low fields.

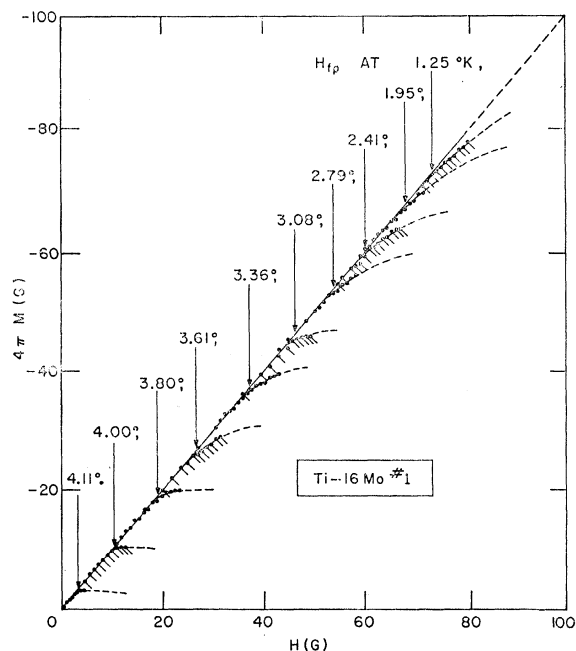


FIG. 2. Low-field isothermal superconducting magnetization M versus applied field H for Ti (16 at. % Mo) No. 1. For clarity only data taken in increasing H ($H \uparrow$) near the initial-flux-penetration field $H_{fp}(T)$ are shown, alternately with and without ticks for successive measurement temperatures T . The bending over of the superconducting $M_s(H \uparrow)$ away from the 45° -slope line of perfect diamagnetism signals the entry of flux into the specimen and determines H_{fp} . In these low fields $M_s(H)$ is irreversible and $M_s(H \downarrow)$ (not shown) consists of a nearly 45° -slope line whose displacement from the origin is determined by the small increasing-field excursion ΔH beyond H_{fp} . To avoid residual-applied-field complications, the measurements were begun at the highest T with the virgin superconducting magnet and ΔH was kept small as shown in the figure. Trapped flux in the specimen was eliminated after each H_{fp} determination by warming the specimen above T_c and then cooling to the measurement temperature in essentially zero H .

⁶² T. G. Berlincourt, Phys. Rev. **114**, 969 (1959).

⁶³ R. R. Hake, D. H. Leslie, and T. G. Berlincourt, Phys. Rev. **127**, 170 (1962).

⁶⁴ J. O. Linde, in *Proceedings of the Fifth International Conference on Low-Temperature Physics and Chemistry*, edited by J. R. Dillinger (University of Wisconsin Press, Madison, Wisconsin, 1958), p. 402.

⁶⁵ The 0.006-in. diam insulated Au(0.07 at. % Fe) wire was obtained from Engelhard Industries, Inc., Baker Platinum Division.

⁶⁶ R. Berman and D. J. Huntley, Cryogenics **3**, 70 (1963); R. Berman, J. C. F. Brock, and D. J. Huntley, *ibid.* **4**, 233 (1964); D. K. Finnemore, J. E. Ostenson, and T. F. Stromberg, Ames Laboratory Report No. IS-1046, 1964 (unpublished).

⁶⁷ J. P. Frank and D. L. Martin, Can. J. Phys. **39**, 1320 (1961).

⁶⁸ R. Radebaugh and P. H. Keesom, Phys. Rev. **149**, 209 (1966).

⁶⁹ J. I. Budnick, Phys. Rev. **119**, 1578 (1960).

The paramagnetic $M_n(H)$ characteristic was determined from magnetization measurements in the normal state outside the $H_u(T^2)$ boundary of Fig. 6. The $M_n(H)$ line appeared to be reversible and temperature independent in the range of measurement $1.86 < T < 4.2^\circ\text{K}$, and indicated $\chi_n \equiv M_n(H)/H = 1.8 \times 10^{-5}$ emu cm^{-3} , a value typical of localized-moment-free bcc transition metals in the present range of conduction-electron-to-atom ratio. As is usual in transition metals and alloys, the measured χ_n is considerably larger than the Pauli spin susceptibility $\chi_P(N)$ calculated from the specific-heat-indicated density of states N (see Table II, Nos. 4 and 5). The difference may be due primarily to the presence of orbital paramagnetism,⁷⁰⁻⁷² although conduction-electron exchange and correlation effects on

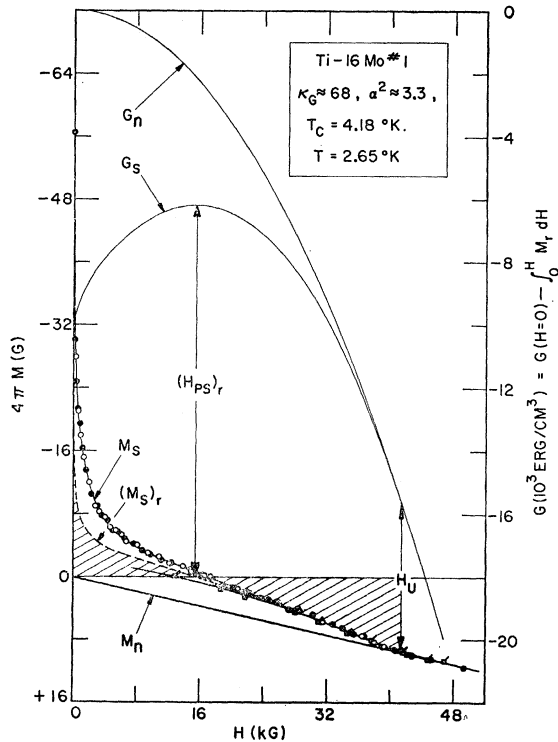


FIG. 3. Magnetization M versus applied magnetic field H for Ti(16 at.% Mo) No. 1 at $T=2.65^\circ\text{K}$. Black and white data points were taken on different days. Square points with ticks were taken on the return decreasing- H cycle. The reversible superconducting magnetization curve $(M_s)_r$ and the Gibbs free energies $G_s(H)$ and $G_n(H)$ are constructed with the help of the specific-heat data of Ref. 45 as explained in the text. The upper critical field H_u (2.65°K) is determined by the contact point of the $G_s(H)$ and $G_n(H)$ curves.

⁷⁰ R. Kubo and Y. Obata, J. Phys. Soc. Japan **11**, 547 (1956); R. Kubo, in *Lectures in Theoretical Physics*, 1965, edited by W. E. Brittin (University of Colorado Press, Boulder, Colorado, 1966), Vol. VIIIa, p. 239.

⁷¹ A. M. Clogston, A. C. Gossard, V. Jaccarino, and Y. Yafet, Phys. Rev. Letters **9**, 262 (1962).

⁷² A. M. Clogston, A. C. Gossard, V. Jaccarino, and Y. Yafet, Rev. Mod. Phys. **36**, 170 (1964).

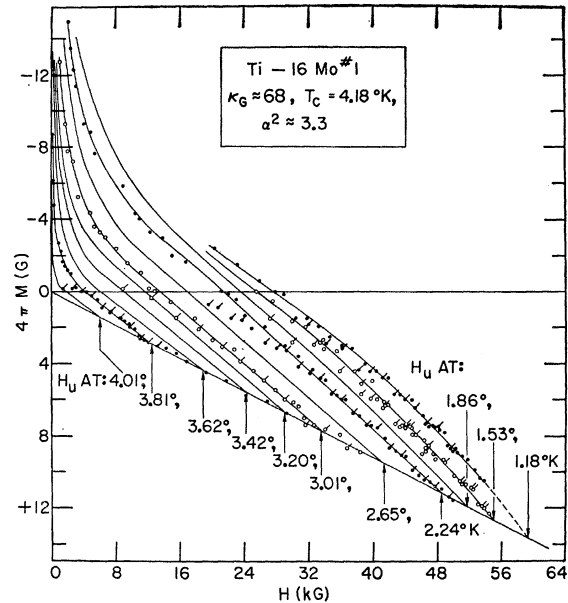


FIG. 4. Isothermal magnetization M versus applied magnetic field H for Ti(16 at.% Mo) No. 1. For clarity only data points for $T=3.81, 3.01, 2.24, 1.53,$ and 1.18°K have been shown. The points with ticks were obtained on the return decreasing- H cycle. Note the reversibility in the high-field paramagnetic mixed-state region, and the convexity of the high-field, low-reduced-temperature magnetization curves. The lower slanted line on which the arrows terminate is the normal-state magnetization characteristic $M_n(H)$ and implies a low-temperature normal-state susceptibility $\chi_n(4.2^\circ\text{K}) \equiv M_n(H)/H = 1.8 \times 10^{-5}$ emu cm^{-3} .

the susceptibility⁷³⁻⁷⁴ and possible phonon enhancement⁷⁵ of the apparent electronic-specific-heat coefficient (and thus N) should also be considered.

Figure 3 shows, in addition to the measured $M_s(H)$ and $M_n(H)$ curves at 2.65°K , a curve $(M_s)_r$ which approximates the reversible superconducting magnetization curve at that temperature. Equating the Gibbs free energies of superconducting and normal phases at the transition field H_u yields, for any given T ,

$$\Delta G_{ns}(H=0) \equiv G_n(H=0) - G_s(H=0) \equiv H_c^2/8\pi$$

$$= \int_0^{H_u} M_n(H) dH - \int_0^{H_u} M_{sr}(H) dH, \quad (1)$$

where M_{sr} is the reversible component of M_s . The thermodynamic critical field for Ti(16 at.% Mo) No. 1 at the temperature of interest,

$$H_c(T=2.65^\circ\text{K}) = 514 \text{ G}, \quad (2)$$

is obtained from the calorimetrically⁴⁵ deduced

⁷³ For a recent review see C. Herring, *Magnetism*, edited by G. T. Rado and H. Suhl (Academic Press Inc., New York, 1966), Vol. IV.

⁷⁴ N. F. Berk and J. R. Schrieffer, Phys. Rev. Letters **17**, 433 (1966).

⁷⁵ A. M. Clogston, Phys. Rev. **136**, A8 (1964); N. W. Ashcroft and J. W. Wilkins, Phys. Letters **14**, 285 (1965).

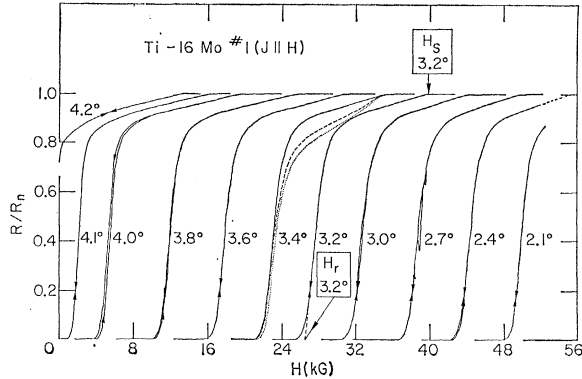


FIG. 5. X-Y recorder tracings of isothermal resistance R divided by the normal-state resistance R_n versus applied field H for Ti(16 at. % Mo) No. 1. The solid curves are for a current density $J=3\text{A}/\text{cm}^2$. The field H is parallel to both J and the longitudinal axis of the specimen. The 3.2°K curve indicates the way in which the resistively measured upper critical field H_r and the sheath upper critical field H_s are arbitrarily defined at $J=3\text{A}/\text{cm}^2$. At 3.4°K the dashed and dotted curves are for $J=0.3$ and $0.15\text{A}/\text{cm}^2$, respectively, and show that both H_r and H_s (but not the sheath resistance) are independent of J for $0.15 \leq J \leq 3\text{A}/\text{cm}^2$.

$H_c(T=0) \equiv H_{c0} = 890\text{G}$ of Table II, No. 14a. It is assumed that the deviation function

$$D(t) \equiv [H_c(t)/H_{c0}] - (1-t^2) \quad (3)$$

(where the reduced temperature $t \equiv T/T_c$) for Ti(16 at. % Mo) No. 1 is identical to the weak-coupling In-type⁷⁶ $D(t)$ which was calorimetrically measured⁴⁵ for another specimen of Ti(16 at. % Mo). [Only an upper limit⁴¹ to $H_c(T)$ can be obtained from the areas between $M_n(H)$ and the irreversible-in-low- H $M_s(H)$ magnetization curves of Fig. 4 (see Table II, No. 14b).] The curve $(M_s)_r$ at $T=2.65^\circ\text{K}$ is then constructed so as to (a) satisfy Eqs. (1) and (2), and (b) coincide with the measured $M_s(H)$ in the high-field region where $M_s(H)$ is reversible. The superconducting- and normal-state free energies, $G_s(H)$ and $G_n(H)$, can then be derived from the reversible $(M_s)_r$ and M_n in accord with the standard relationship between magnetization and free energy indicated along the right-hand ordinate of Fig. 3, and the zero-field free-energy difference $\Delta G_{ns}(H=0)$ of Eqs. (1) and (2). The extreme type-II $G(H)$ curves of Fig. 3 are quite different from those calorimetrically derived⁷⁷ for V(5 at. % Ta), a standard low- κ_G , low- H_u , type-II superconductor for which neither $M_s(H)$ nor $M_n(H \leq H_u)$ is appreciably paramagnetic. The experimentally indicated $G(H)$ curves of Fig. 3 also show, somewhat more clearly than previously published schematic plots,^{16,29,42} that for the high- κ_G case the position of the second-order-type merging of

the free-energy curves, and hence the magnitude of the upper critical field H_u , is strongly dependent upon the relative degree to which superconducting- and normal-state free energies are lowered by paramagnetism.

The magnetization data of Fig. 4 essentially agree with the earlier measurements⁴¹ at $H \leq 27\text{kG}$, and agree at least qualitatively with the vibrating-sample measurements of Cape⁴² on the same alloy. The present data show (1) reversible high-field mixed-state paramagnetic superconductivity; (2) persistence of the second-order upper critical field to a reduced temperature $t \equiv T/T_c = 1.53^\circ\text{K}/4.18^\circ\text{K} = 0.37$; (3) an extrapolated zero- T upper critical field $H_{u0} \approx 63\text{kG}$ (Fig. 13), in reasonable agreement with the earlier pulsed-field resistive-onset measurements^{15,16} which gave $H_r(1.2^\circ\text{K}) \approx 64\text{kG}$, and markedly lower than the¹⁷ $H_{c20^*} \approx 100\text{kG}$ (Table II, No. 20) predicted by spin-ignoring neo-GLAG theory⁹⁻¹⁴; (4) a decrease of $\kappa_1(T) \equiv H_u(T)/[\sqrt{2}H_c(T)]$ with decrease of T (Fig. 16); and (5) an increase of the relative terminal mixed-state magnetization slope

$$S(T) \equiv \{d[4\pi(M_s - M_n)]/dH\}_{H_u}$$

with decrease of T [corresponding to decreasing $\kappa_2(T)$ with decrease of T (Fig. 17)].

The curves of Fig. 4 show linearity of $M_s(H_{ps} \leq H \leq H_u)$ in the high- t region [also shown in the previous ballistic magnetization measurements on Ti(16 at. % Mo)⁴¹ and in Figs. 7, 9, and 10], and convexity of $M_s(H_{ps} \leq H \leq H_u)$ in the low- t region. Presumably the shape change reflects a trend towards

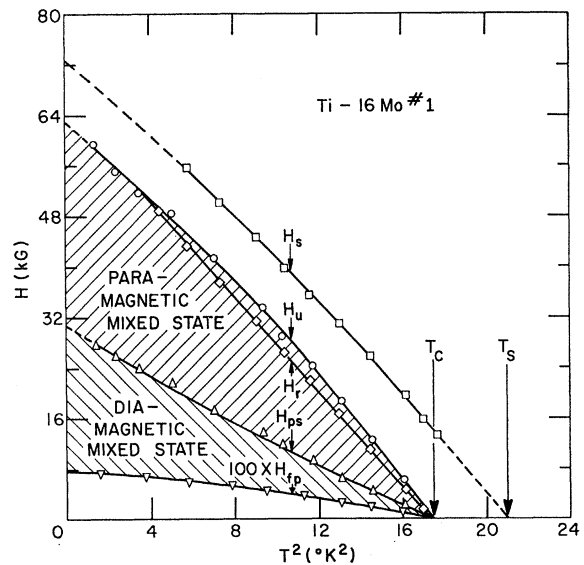


FIG. 6. The $(H-T)$ phase diagram of Ti(16 at. % Mo) No. 1. Here H_{fp} is the initial-flux-penetration field (Fig. 2), H_{ps} is the paramagnetic-superconductivity onset field where the mixed-state magnetization curve crosses the zero- M axis (Fig. 4), H_r is the resistively measured upper critical field (Fig. 5), H_u is the magnetization-measured upper critical field (Fig. 4), and H_s is the resistively determined sheath upper critical field (Fig. 5).

⁷⁶ R. W. Shaw, D. E. Mapother, and D. C. Hopkins, Phys. Rev. **120**, 88 (1960).

⁷⁷ R. R. Hake and W. G. Brammer, Phys. Rev. **133**, A719 (1964); R. R. Hake, Rev. Mod. Phys. **36**, 124 (1964). Magnetization measurements by R. R. Hake and L. J. Barnes (unpublished) on annealed V(5 at. % Ta) show nearly ideal reversible low- κ_G type-II behavior except near H_{c1} .

a first-order transition at low t where quasiparticle excitations are reduced.

Figure 5 shows normalized resistance versus longitudinal applied field H at various temperatures for the same Ti(16 at.% Mo) specimen on which the magnetization measurements were made. As indicated for the 3.2°K curve, there is a fairly abrupt onset of resistance near the arbitrarily defined resistively measured upper critical field H_r . Note the long resistive tail intersecting the normal-state resistance curve at the field H_s . The sensitivity of this tail to current density (shown in the 3.4°K curves) and copper plating⁴⁷⁻⁴⁹ suggests that H_s is a *sheath* upper critical field.

Figure 6 shows the (H - T) phase diagram for Ti(16 at.% Mo) No. 1 as determined by the present measurements. The mixed state is divided into diamagnetic and paramagnetic regions. The resistively measured upper critical field $H_r(T^2)$ is close to the magnetization-determined upper critical field $H_u(T^2)$, thus reinforcing the present concept of paramagnetic superconductivity. Specific-heat determinations⁴⁵ of $H_u(T^2)$, not shown in Fig. 6, extending up to 29 kG on a different specimen of Ti(16 at.% Mo), show reasonable agreement with the magnetization-determined $H_u(T^2)$ boundary. The initial flux penetration field $H_{fp}(T^2)$ is a factor two to four higher than the $H_{c1}(T^2)$ predicted by theory^{19,27,78} (see also Table II, No. 19), probably related to the low-field irreversibility of the present specimen. Figure 6 shows that H_{fp}

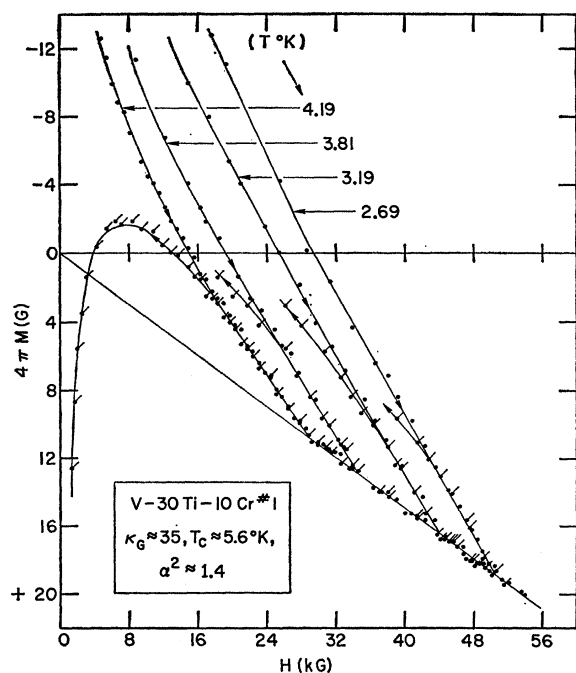


FIG. 7. Isothermal magnetization M versus applied magnetic field H for V(30 at.% Ti)(10 at.% Cr) No. 1. The points with ticks were obtained on the return decreasing- H cycle.

⁷⁸ J. L. Harden and V. Arp, *Cryogenics* **3**, 105 (1963).

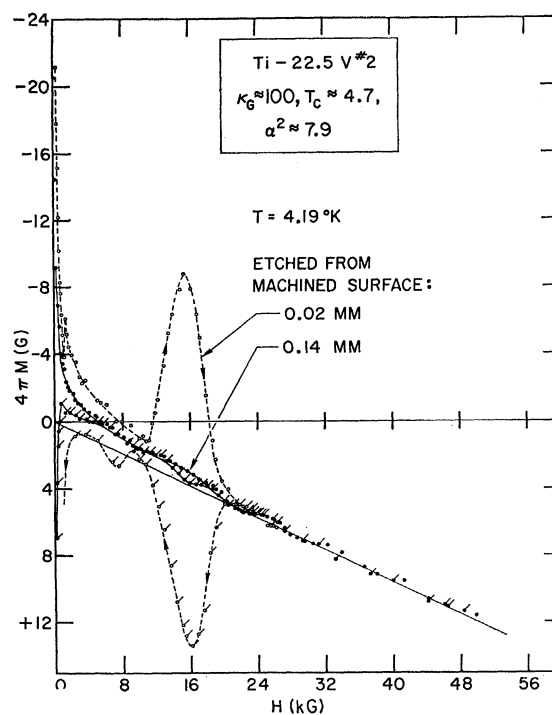


FIG. 8. Isothermal magnetization M versus applied magnetic field H for Ti(22.5 at.% V) No. 2, measured at 4.19°K before and after heavy chemical etching. The points with ticks were obtained on the return decreasing- H cycle. The large irreversible peak effect in the magnetization centered at 16 kG is apparently associated with surface defects as discussed in the text.

is not parabolic in T as reported by Blaugher⁶ for some highly irreversible Ti-V alloys. The sheath critical field $H_s(T^2)$ and the sheath's higher-than-bulk transition temperature T_s are discussed elsewhere.^{48,49} The high-field reversibility of $M_s(H)$ and the fair agreement of H_u values as determined by magnetization and calorimetric measurements⁴⁵ indicate that the sheath on annealed and chemically etched (polished) Ti(16 at.% Mo) has too low a critical current to seriously affect the magnetization. The current-density independence of the resistive-onset field (Fig. 5) and temperature (Sec. III.D) at $0.3 \leq J \leq 3$ A/cm² [corresponding for the present specimens to $0.011 \leq J$ (surface) ≤ 0.11 A/cm] also indicates low sheath critical current. This low sheath critical current is presumably associated with relatively small sheath thickness $\approx \xi_G \approx 56(1-t)^{-1/2}$ (Table II, No. 24), where ξ_G is in Å.

B. V(30 at.% Ti)(10 at.% Cr)

Figure 7 shows isothermal magnetization curves for the annealed specimen V(30 at.% Ti)(10 at.% Cr) No. 1. Photomicrographs representative of this specimen showed a precipitate concentration about half that shown in Fig. 1(c) and existing in a somewhat less disbursed form. The $M_s(H)$ curves are qualitatively similar to those of Fig. 4, with reversibility only in the high-field paramagnetic mixed-state region. As for

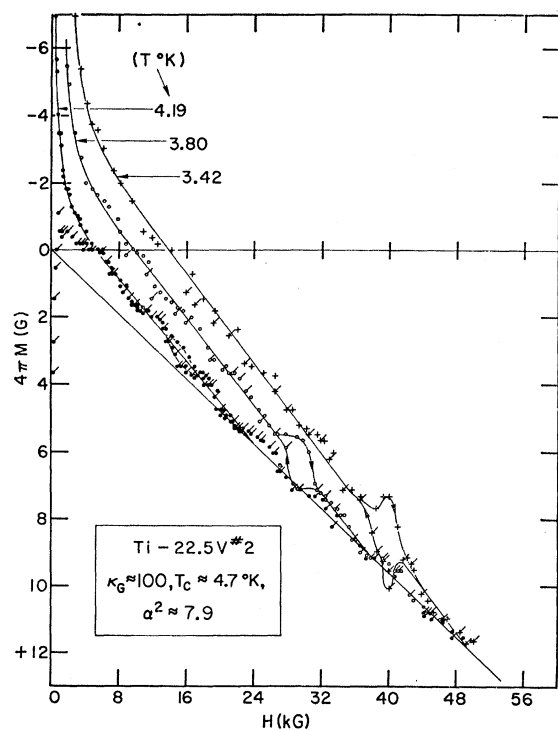


FIG. 9. Isothermal magnetization M versus applied magnetic field H for Ti(22.5 at.% V) No. 2 after the heavy etching indicated in Fig. 8. The points with ticks were obtained on the return decreasing- H cycle.

Ti(16 at.% Mo) No. 1, $S(T)$ increases with decrease of T . The helium-temperature normal-state susceptibility as determined by the $M_n(H)$ measurements of Fig. 7 is $\chi_n(4.2^\circ\text{K}) = 3.0 \times 10^{-5} \text{ emu cm}^{-3}$.

C. Ti(22.5 at.% V)

Figures 8 and 9 show isothermal magnetization curves for the unannealed specimen Ti(22.5 at.% V) No. 2. Photomicrographs representative of this specimen are similar to Fig. 1(b). The large irreversible "peak effect" centered at 16 kG in Fig. 8 is apparently associated with surface defects (probably produced by the machining operation), since further chemical etching nearly eliminated the peak effect as shown in the figure. Figure 9 shows that the small residual peak effect which remains after heavy etching moves to higher field and becomes more pronounced as temperature is reduced. Peak effects in magnetization curves have also been observed (in much less prominent form than in Fig. 8) by Livingston⁷⁹ in Pb-In alloys and are associated^{49,79} with the more well-known and interrelated⁸⁰ "peak effect" in critical current den-

⁷⁹ J. D. Livingston, Phys. Rev. **129**, 1943 (1963); Rev. Mod. Phys. **36**, 54 (1964). N. Tsuda, S. Kolke, and T. Suzuki [Phys. Letters **22**, 412 (1966)] have reported a peak effect in dB/dH versus H in Nb.

⁸⁰ T. G. Berlincourt, R. R. Hake, and D. H. Leslie, Phys. Rev. Letters **6**, 671 (1961); R. R. Hake, T. G. Berlincourt, and D. H. Leslie, Bull. Am. Phys. Soc. **7**, 474 (1962).

sity^{80,81} and "dip effect" in transverse-field mixed-state resistance.^{62,80,82} Apparently the high-field impedance to flux motion presented by the surface of the present specimen increases with decrease of T and for all T is greatest just below the upper critical field.

Except for the peak effect, the $M_s(H)$ curves of Figs. 8 and 9 are qualitatively similar to those previously discussed for Ti(16 at.% Mo) No. 1 and V(30 at.% Ti) (10 at.% Cr) No. 1, showing the usual reversible paramagnetic mixed-state magnetization and the usual increase of $S(T)$ with decrease of T . The helium-temperature normal-state susceptibility as determined by the $M_n(H)$ measurements of Figs. 8 and 9 is $\chi_n(4.2^\circ\text{K}) = 1.9 \times 10^{-5} \text{ emu cm}^{-3}$.

D. Ti(25 at.% V)

Figure 10 shows paramagnetic mixed-state magnetization curves for the various Ti(25 at.% V) specimens of Table I, all measured at $T = 4.19^\circ\text{K}$. The peak position in the cold-rolled specimen Ti(25 at.% V) No. 2 curve suggests that $H_u(4.19^\circ\text{K}) \approx 52 \text{ kG}$, higher than the earlier reported⁴¹ $\approx 36 \text{ kG}$ which was estimated from magnetization data at $H < 27 \text{ kG}$. The present H_u value implies, from Fig. 10(b), a normal-state suscepti-

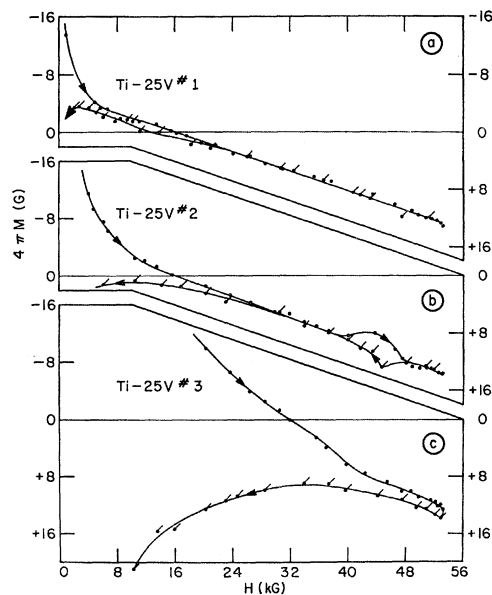


FIG. 10. Isothermal magnetization M versus applied magnetic field H at $T = 4.19^\circ\text{K}$ for Ti(25 at.% V) specimens; No. 1 [as arc cast with no precipitate as shown in Fig. 1(b)], No. 2 (cold rolled to a reduction of $\approx 2:1$), and No. 3 [annealed and containing an annealing-induced precipitate as shown in Fig. 1(c)]. The κ_g , α^2 , and T_c values are listed in Table I.

⁸¹ M. A. R. Le Blanc and W. A. Little, in *Proceedings of the Seventh International Conference on Low-Temperature Physics*, edited by G. M. Graham and A. C. Hollis Hallet (University of Toronto Press, Toronto, 1961), p. 362.

⁸² S. H. Autler, E. S. Rosenblum, and K. H. Goen, Phys. Rev. Letters **6**, 489 (1962).

bility⁸³ $\chi_n(4.2^\circ\text{K}) = 2.0 \times 10^{-5}$ emu cm^{-3} , and a $\kappa_2(4.19^\circ\text{K}) = 61$ from Eq. (12), as plotted in Fig. 19. The peak effect shown for Ti(25 at. % V) No. 2 is again probably associated primarily with surface defects. Similar magnetization peak effects in cold-rolled specimens of Ti(25 at. % V) have been observed⁴⁹ to change in magnitude and shape with etching, presumably as different cold-work-induced defect characteristics are brought to the specimen surface. Comparison of the $M_s(H)$ curves for Ti(25 at. % V) No. 2 (cold-rolled) and Ti(25 at. % V) No. 3 [annealed but containing precipitates as shown in Fig. 1(c)] shows that in the present case precipitates are more effective flux pinners than are the dislocations produced by cold working to a thickness reduction of $\approx 2:1$.

V. DISCUSSION

A. Qualitative Significance

The qualitative significance of paramagnetic superconducting magnetization can be discussed with reference to Fig. 11. This figure contrasts schematic zero-temperature reversible magnetization curves for type-I, "standard" type-II, and extreme type-II superconductors with typical transition-metal electronic properties somewhat similar to, respectively, Ta,⁸⁴ V(5 at. % Ta),⁷⁷ and the Ti(16 at. % Mo) of the present study. The three prototype superconductors have the same superconducting transition temperature T_c and the same zero-temperature superconductive condensation energy $\Delta G_{ns}(H=0, T=0) \equiv H_{c0}^2/8\pi$. Their relevant normal-state electronic parameters are also identical (specifically the parameters listed in Table II, Nos. 2 to 7), except that the low-temperature normal-state electrical resistivities ρ_n differ in the approximate ratio 0.1:10:100, producing the near factor of ten changes in the Gor'kov-Goodman-calculated [Eq. (A13c)] κ_G values shown in the figure. Since the $\Delta G_{ns}(H=0, T=0)$ values are all equal, the cross-hatched condensation-energy areas between the $M_s(H)$ and $M_n(H)$ curves must be equal by Eq. (1). Furthermore, since the $4\pi M$ and H axes have been scaled in opposite sense by successive factors of ten, the cross-hatched areas all appear equal in Fig. 11.

For the extreme type-II superconductor of Fig. 11, the superconductive magnetization $M_s(H)$ must be weak and comparable to the weak paramagnetic magnetization $M_n(H)$ of the normal state if the area enclosed by the M_s and M_n curves is to yield the proper condensation energy. The magnetization $M_n(H)$ is due in part to Pauli electron-spin polarization in the normal

⁸³ This value is somewhat lower than the $\chi_n(295^\circ\text{K}) = 2.5 \times 10^{-5}$ emu cm^{-3} reported for bcc Ti(25 at. % V) by S. Taniguchi, R. S. Tebble, and D. E. G. Williams, Proc. Roy. Soc. (London) **265**, 502 (1962).

⁸⁴ J. Buchanan, G. K. Chang, and B. Serin, J. Phys. Chem. Solids **26**, 1183 (1965).

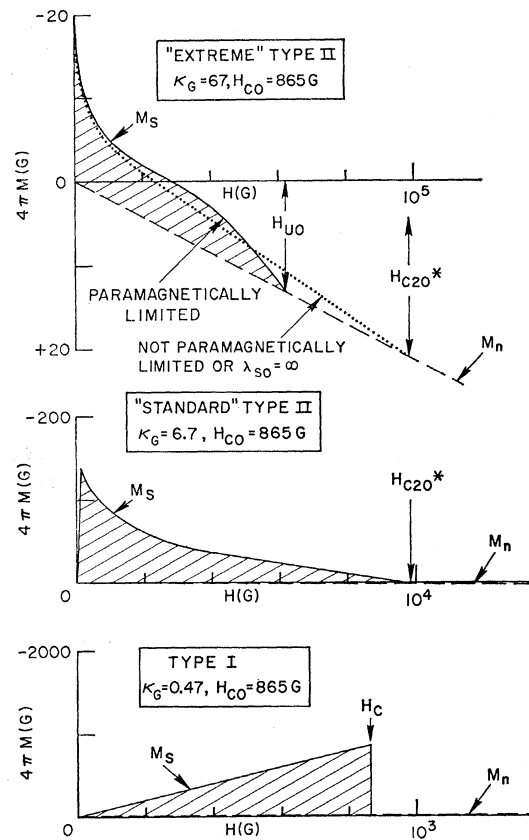


FIG. 11. Schematic zero-temperature reversible magnetization curves for type-I, "standard" type-II, and "extreme" type-II superconductors with typical transition-metal electronic properties as discussed in the text.

state along the applied field. [Orbital paramagnetism⁷⁰⁻⁷² probably also contributes to $M_n(H)$, and should contribute almost equally to $M_s(H)$.^{71,72}] The superconducting magnetization $M_s(H)$ must likewise be partly determined by the amount of Pauli electron-spin polarization in the mixed state, presumably related to the spatial average of the position-, temperature-, and field-dependent quasiparticle density of states characterizing the mixed-state vortex structure, and the fact that opposite spin-coupled Cooper pairs (or, more correctly, dirty-superconductor time-reversed pairs^{8,85}) can exhibit no net spin polarization.⁸⁶

For simplicity, two limiting cases of zero-temperature superconductive electron-spin behavior can be considered:

(1) If Cooper spin pairing were somehow removed without otherwise affecting superconductivity, then Pauli-paramagnetic contributions to $M_s(H)$ and $M_n(H)$ would be nearly equal, and paramagnetism would have little effect on the super-normal free-energy balance. In this case the electron-spin-ignoring dirty-

⁸⁵ D. C. Mattis and J. Bardeen, Phys. Rev. **111**, 412 (1958).

⁸⁶ K. Yosida, Phys. Rev. **110**, 769 (1958).

limit neo-GLAG theory⁹⁻¹⁴ would apply, predicting the linear GLAG-type magnetization curve shown by the dotted line in the top plot of Fig. 11. This curve terminates with relatively low S , or high $\kappa_2(T=0) \approx 1.2\kappa_G$, in a second-order transition to the normal state at the high upper critical field H_{c20}^* with a high $\kappa_1(T=0) \approx 1.2\kappa_G$. [It is clear⁸⁶ that this spin-decoupled regime must always be approached as $T \rightarrow T_c$, quasiparticle excitations increase, and the superconductive order parameter approaches zero. Hence, near T_c , electron-spin-ignoring neo-GLAG theory⁹⁻¹⁴ should always apply such that $\kappa_1(T \rightarrow T_c) = \kappa_2(T \rightarrow T_c) = \kappa_G$.]

(2) On the other hand, if Cooper spin pairing were complete at $T=0$ (even within vortex cores and in the "gapless" region near the upper critical field), then Pauli paramagnetism would not contribute to $M_s(H)$ and we would expect a much less paramagnetic $M_s(H)$ (not necessarily diamagnetic because of the possible orbital-paramagnetic⁷⁰⁻⁷² contribution). In addition, preferential Pauli-paramagnetic lowering of the normal-state free energy would result in an abrupt *first-order* transition to the normal state at a relatively low upper critical field $H_{u0} \ll H_{c20}^*$ with a low $\kappa_1(T=0) \ll 1.2\kappa_G$ (since the condensation energy area must be conserved). In this case, conduction electrons would suddenly depart at the upper critical field in order to take energetic advantage of spin alignment along H , thus producing a *discontinuity* ($S \rightarrow \infty$, $\kappa_2 \rightarrow 0$) in the magnetization curve. (We ignore here the possibility of a Fulde-Ferrell⁸⁷⁻⁸⁹ state.) A first-order transition to the normal state in the paramagnetically limited case was first envisaged by Clogston.²³

The actual extreme type-II magnetization curves of this study represent a compromise between the limiting cases discussed above. At low reduced temperatures, where quasiparticle excitations are reduced and the effects of Cooper spin coupling should be most apparent,⁸⁶ the curves of Fig. 4 are similar to the solid curve labelled " M_s " and "paramagnetically limited" at the top of Fig. 11. Despite the paramagnetic limitation, the observed second-order transition shows that there must be considerable Pauli spin polarization contributing to $M_s(H)$, especially near the upper critical field. In fact, the recent WHH²⁹ and Maki²⁸ spin-effect theories imply that magnetization curves such as those of Fig. 4, with relatively low- S , second-order transitions at low reduced temperature, can result from an enhancement of mixed-state Pauli paramagnetism by spin-orbit-coupling-induced electronic spin-flip scattering.

As first pointed out by Ferrell⁹⁰ and Anderson⁹¹ with reference to the superconductive Knight shift, such scattering effectively acts to decouple spin pairing⁹⁰⁻⁹³ (but not time-reverse pairing^{8,85}) of one-electron wave functions appropriate to the strong nonmagnetic scattering case.^{8,85} Both the WHH and the Maki theories suggest that the dotted GLAG-type magnetization curve at the top of Fig. 11 would be approached at low t for nearly complete spin decoupling of time-reverse pairs, resulting from a high spin-flip scattering frequency, proportional to the WHH²⁹ spin-orbit parameter λ_{so} .

B. The WHH and Maki Theories

WHH²⁹ and Maki²⁸ have independently found solutions to the linearized Gor'kov equations²⁰⁻²² in the dirty limits ($\xi_0 \gg l$, see Table II, No. 33), which is applicable to the present alloys, taking into account both Pauli paramagnetism and spin-orbit-coupling induced electronic spin-flip scattering. According to the theories, the reduced upper critical field

$$h^*(t) \equiv H_{c2}(t)/(-dH_{c2}/dt)_{t=1} \quad (4)$$

is determined by the Maki paramagnetic limitation parameter α , and the adjustable spin-flip scattering frequency parameter λ_{so} . The theories also yield the relationship

$$0.693(-dH_{c2}/dt)_{t=1} = H_{c20}^*, \quad (5)$$

where H_{c20}^* is the dirty-limit neo-GLAG upper critical field in the absence of paramagnetic limitation. The λ_{so} independence of $(dH_{c2}/dt)_{t=1}$ [and the related $\kappa_1(t \rightarrow 1) = \kappa_2(t \rightarrow 1) = \kappa_G$] is associated with the fact that the paramagnetic limitation on H_{c2} must vanish as $t \rightarrow 1$, the spatial average of the superconductive order parameter approaches zero, and the Pauli spin susceptibility of the superconducting mixed state approaches that of the normal state. Substitution of Eq. (5) in Eq. (4) yields

$$h^*(t) = 0.693H_{c2}(t)/H_{c20}^*. \quad (6)$$

Since H_{c20}^* can be calculated in the dirty limit from measured normal-state electronic parameters by Eq. (A16b), Eqs. (4) and (6) both afford experimental definition of $h^*(t)$.

Alternatively, the theories yield upper-critical-field predictions in terms of the parameter

$$\kappa_1^*(t) \equiv \kappa_1(t)/\kappa_1(t=1), \quad (7)$$

⁹⁰ R. A. Ferrell, Phys. Rev. Letters **3**, 262 (1959).

⁹¹ P. W. Anderson, Phys. Rev. Letters **3**, 325 (1959); in *Proceedings of the Seventh International Conference on Low-Temperature Physics*, edited by G. M. Graham and A. C. Hollis Hallet (University of Toronto Press, Toronto, 1961), p. 298.

⁹² A. A. Abrikosov and L. P. Gor'kov, Zh. Eksperim. i Teor. Fiz. **42**, 1088 (1962) [English transl.: Soviet Phys.—JETP **15**, 752 (1962)].

⁹³ P. Fulde and K. Maki, Phys. Rev. **139**, A788 (1965); J. Appel, Phys. Rev. **139**, A1536 (1965).

⁸⁷ P. Fulde and R. A. Ferrell, Phys. Rev. **135**, A550 (1964); A. I. Larkin and Y. N. Ovchinnikov, Zh. Eksperim. i Teor. Fiz. **47**, 1136 (1964) [English transl.: Soviet Phys.—JETP **20**, 762 (1965)].

⁸⁸ L. W. Gruenberg and L. Gunther, Phys. Rev. Letters **16**, 996 (1966).

⁸⁹ R. Avenhaus and P. Fulde, Physik Kondensierten Materie **5**, 157 (1966).

where

$$\kappa_1(t) \equiv H_{c2}(t)/[\sqrt{2}H_c(t)] \quad (8)$$

and $H_c(t)$ is the thermodynamic critical field. From Eqs. (6)–(8), and (A16a), and the dirty-limit $\kappa_1(0^\circ\text{K})/\kappa_1(t=1) = 1.195$,¹² it follows that⁹⁴

$$\kappa_1^*(t) = 1.73[H_{c0}/H_c(t)]h^*(t). \quad (9)$$

In terms of the deviation function $D(t)$ of Eq. (3), Eq. (9) becomes

$$\kappa_1^*(t) = 1.73[D(t) + (1-t^2)]^{-1}h^*. \quad (10)$$

As emphasized by Helfand and Werthamer,¹² the comparison of experiment and theory in terms of κ_1^* can be misleading, especially near $t=1$, unless $D(t)$ and $H_c(t)$ for the particular specimen in question are known. These can be obtained for type-II superconductors from (1) double integration of zero-field specific-heat data,^{45,68,77} or (2) the area between *reversible* normal- and superconducting-state magnetization curves [see Eq. (1)].

Assuming the existence of an Abrikosov¹⁹ vortex lattice, Maki²⁸ has also deduced the behavior of the terminal mixed-state magnetization slope parameter,

$$\kappa_2^*(t) \equiv \kappa_2(t)/\kappa_2(t=1), \quad (11)$$

in terms of α and λ_{so} . Here $\kappa_2(t)$ is defined by

$$S(t) \equiv \{d[4\pi(M_s - M_n)]/dH\}_{H_{c2}} = \{[2\kappa_2^2(t) - 1]\beta\}^{-1}, \quad (12)$$

where $\beta = 1.16$ for a triangular vortex lattice.⁹⁵

The paramagnetic limitation parameter²⁸ is

$$\alpha \equiv \sqrt{2}H_{c20}^*/H_{p0}, \quad (13)$$

where H_{p0} is the zero-temperature upper-critical-field limit given by Clogston's²³ Eq. (A17b). In general, and as previously shown experimentally for several high- κ_G alloy systems,^{15,16} the higher the value of $\alpha \propto H_{c20}^*/H_{p0}$, the lower will be the value of $h^* \propto H_{c2}(t)/H_{c20}^*$. The α parameter can be calculated in the dirty limit from normal-state electronic parameters by Eq. (A18b), or from the slope of the upper-critical-field curve near T_c by Eq. (A18c).

A necessary condition for the observation of mixed-state paramagnetism over a wide field range in transition-metal-alloy superconductors can be written in terms of α : Comparing the extreme and standard type-II magnetization curves of Fig. 11 it can be seen that the area $\frac{1}{2}\chi_n(H_{c20}^*)^2$ enclosed by the paramagnetic normal-state magnetization curve should be approximately equal to or greater than the condensation-energy area $H_{c0}^2/8\pi = \frac{1}{2}\chi_P H_{p0}^2$ [where the last

⁹⁴ Equation (9) was derived by N. R. Werthamer, E. Helfand, and P. C. Hohenberg (private communication).

⁹⁵ W. H. Kleiner, L. M. Roth, and S. H. Autler, Phys. Rev. **133**, A1226 (1964); J. Matricon, Phys. Letters **9**, 289 (1964); D. Cribier, B. Jacrot, L. Madhav Rao, and B. Farnoux, Phys. Letters **9**, 109 (1964); W. Fite, II, and A. G. Redfield, Phys. Rev. Letters **17**, 381 (1966).

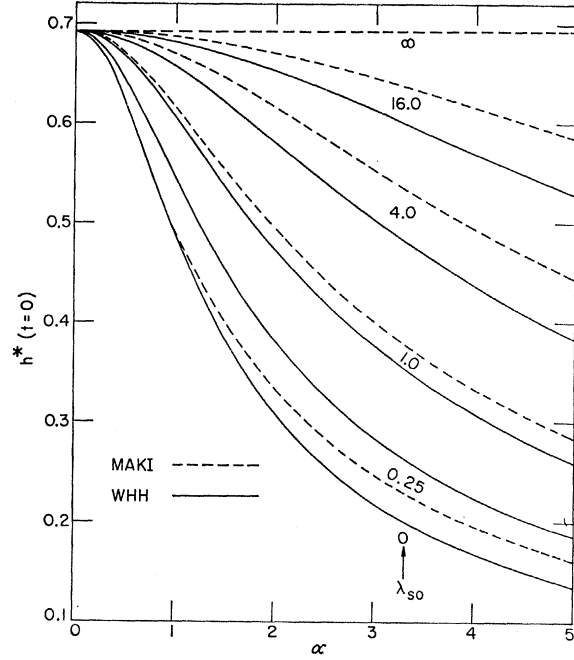


FIG. 12. The reduced upper critical field in the dirty limit at zero temperature $h^*(t=0) \equiv H_{c20}/(-dH_{c2}/dt)_{t=1} = 0.693H_{c20}/H_{c20}^*$ versus the Maki paramagnetic limitation parameter $\alpha \equiv \sqrt{2}H_{c20}^*/H_{p0} = 2.35\rho_n\gamma$ for various values of the spin-orbit-scattering frequency parameter λ_{so} according to the theories of Maki (Ref. 28) and WHH (Ref. 29). The dashed Maki curves are derived from Eqs. (25) and (26) of the text, and the solid WHH curves are derived by computer solution of Eq. (28) of Ref. 29.

equality follows from Eq. (A17a)]. Thus the necessary condition is $\chi_n(H_{c20}^*)^2 \gtrsim \chi_P H_{p0}^2$, or assuming a reasonable $\chi_n \approx 2\chi_P$, $2(H_{c20}^*)^2/H_{p0}^2 \equiv \alpha^2 \gtrsim 1$.

The spin-flip-scattering frequency parameter is²⁹

$$\lambda_{so} \equiv \hbar(3\pi k_B T_c \tau_{so})^{-1}, \quad (14)$$

where \hbar and k_B have their usual meanings and τ_{so} is the mean spin-flip scattering time. For a dirty superconductor,^{8,72} the electronic spin quantum number should become undefined, spin coupling of electrons in mutually time-reversed states should be at least partially removed, and mixed-state paramagnetism should be enhanced (thus h^* increased), when the energy uncertainty $\Delta E \approx \hbar\tau_{so}^{-1}$ becomes greater than the BCS^{96,97} energy gap

$$2\Delta_{00} = 3.52k_B T_c; \quad (15)$$

or equivalently from Eq. (14) when

$$\lambda_{so} \geq 0.37, \quad (16)$$

as is indeed borne out by the detailed results of the theories as indicated in Fig. 12.

A condition²⁹ for the application of the WHH and

⁹⁶ J. Bardeen, L. N. Cooper, and J. R. Schrieffer, Phys. Rev. **108**, 1175 (1957).

⁹⁷ J. Bardeen and J. R. Schrieffer, in *Progress in Low-Temperature Physics*, edited by C. J. Gorter (Interscience Publishers, Inc., New York, 1961), Vol. III, p. 170.

Maki theories is the physically realistic requirement that the spin-flip-scattering time τ_{so} be large in comparison with the transport scattering time τ_{tr} . From Eqs. (A4) and (A19) this condition can be written as

$$\lambda_{so} \ll 3.7 \times 10^{-21} \rho_n n^{4/3} (S/S_f)^2 (\gamma T_c)^{-1}, \quad (17)$$

where the symbols and units are as given in the Appendix. With the usual assumption^{16,98,99} $S/S_f=0.6$, Eq. (17) implies that the WHH and Maki theories should be applicable to Ti(16 at.% Mo) No. 1, V(30 at.% Ti) (10 at.% Cr) No. 1, Ti(22.5 at.% V) No. 2, and Ti(25 at.% V) No. 2 if $\lambda_{so} \ll 71, 23, 86,$ and $58,$ respectively. From these examples, the form of Eq. (17), and the curves of Fig. 12, it can be seen that the theories predict a substantial alleviation of the paramagnetic limitation on h^* for real materials of interest ($1 \lesssim \alpha \lesssim 5$) at physically realistic values of λ_{so} . Therefore, in Figs. 12–14 and 16–19, the uppermost theoretical curve is labelled $\lambda_{so} = \infty$ to indicate

$$h^*(\alpha=0, \lambda_{so} \geq 0) = \lim_{\lambda_{so} \rightarrow \infty} h^*(\alpha > 0), \quad (18)$$

$$\kappa_1^*(\beta_0^2=0, \alpha=0, \lambda_{so} > 0) = \lim_{\lambda_{so} \rightarrow \infty, \beta_0^2 \rightarrow 0} \kappa_1^*(\alpha > 0), \quad (19)$$

$$\kappa_2^*(\beta_0^2=0, \alpha=0, \lambda_{so} > 0) = \lim_{\lambda_{so} \rightarrow \infty, \beta_0^2 \rightarrow 0} \kappa_2^*(\alpha > 0), \quad (20)$$

where β_0^2 is given by Eq. (21), even though Eq. (17) will be violated as $\lambda_{so} \rightarrow \infty$. Equations (18)–(20) also seem reasonable in view of the qualitative arguments of Sec. V. A.

Maki²⁸ has obtained approximate expressions for $h^*(t)$, $\kappa_1^*(t)$, and $\kappa_2^*(t)$ in terms only of a parameter

$$\beta_0^2 \equiv \alpha^2 / (1.78 \lambda_{so}), \quad (21)$$

in the region where the spin-flip scattering time is short, i.e.,

$$\tau_{so} \ll \hbar (\Delta_{00})^{-1} \quad (22)$$

or, by substitution of Eqs. (14) and (15),

$$\lambda_{so} \gg 0.2. \quad (23)$$

The validity of Maki's approximate expressions is still subject to Eq. (17), so that the full condition on λ_{so} becomes

$$3.7 \times 10^{-21} \rho_n n^{4/3} (S/S_f)^2 (\gamma T_c)^{-1} \gg \lambda_{so} \gg 0.2. \quad (24)$$

In terms of $h^*(t)$, the approximate Maki expression for the upper critical field is

$$h^*(t) = 1.39 h_{c2} [1 + (1 + \beta_0^2 h_{c2})^{1/2}]^{-1}, \quad (25)$$

⁹⁸ B. B. Goodman, Phys. Rev. Letters **6**, 597 (1961).

⁹⁹ For a recent tabulation of S/S_f for pure metals, see Ref. 4. It is interesting to note that the assumption $S/S_f=1$, together with the assumption that the conduction electrons per atom n_a are those outside closed shells, leads to unrealistically low calculated values of the electron mean free path $l(S/S_f=1) \equiv l_0$ from Eq. (A2) for Ti-V alloys; comparing l_0 and the lattice parameter a in Å: Ti(22.5 at.% V) ($l_0=2.16, a \approx 3.21$), Ti(25 at.% V) ($l_0=2.40, a \approx 3.20$). (For the bcc lattice the nearest-neighbor distance is $\sqrt{3} a/2$.)

where, using Eq. (6),

$$h_{c2} \equiv H_{c2}^*(t) / H_{c20}^* = (0.693)^{-1} h^*(t, \alpha=0, \lambda_{so}=0). \quad (26)$$

Equation (25) is equivalent to the corrected¹⁰⁰ form of Maki's²⁸ Eq. (52) in which the coefficient of τ_{so} is changed from 12^* to 18.

Judging from the presently indicated $0.5 \lesssim \lambda_{so} \leq 1.3$ of Table II, No. 29, the application of the WHH theory is probably justified for the present alloys according to Eq. (17),[†] but the approximate Maki expression for the strong-spin-orbital scattering limit may not be completely applicable according to the right-hand side of Eq. (24).

C. Comparison of Theory and Experiment

1. Ti(16 at.% Mo)

a. Upper Critical Field. Figures 13–15 compare with increasing resolution the present upper-critical-field data with the theories of Maki and WHH. Figures 14 and 15 also show for comparison the vibrating-sample magnetometer data of Cape⁴² on another specimen of Ti(16 at.% Mo) ($T_c=4.1^\circ\text{K}$), and the calorimetric data of Barnes and Hake⁴⁵ in still another specimen ($T_c=4.246^\circ\text{K}$). The T_c variation among these specimens may be due to slightly different alloy or inter-

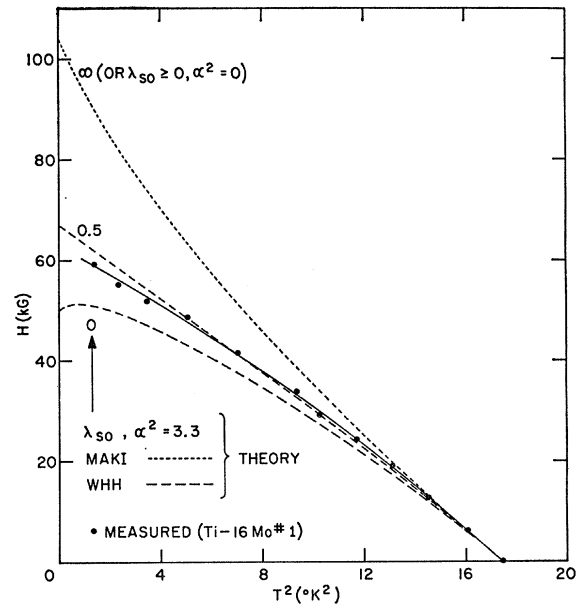


FIG. 13. Upper critical field H_u versus T^2 for Ti(16 at.% Mo) No. 1 as determined by the magnetization data of Fig. 4. The theoretical $H_{c2}(T^2)$ curves are obtained by multiplying the theoretical $h^*(t, \alpha, \lambda_{so}) = H_{c2}(t) / (-dH_{c2}/dt)_{t=1}$ by the experimentally indicated $(-dH_u/dt)_{t=1} = 150$ kG. The Maki $h^*(t, \alpha, \lambda_{so})$ is obtained from Eqs. (25) and (26) of the text. The WHH $h^*(t, \alpha, \lambda_{so})$ is obtained via computer solution of Eq. (28) of Ref. 29. The identification of the condition ($\lambda_{so} = \infty, \alpha^2 = 3.3$) with the condition ($\lambda_{so} \geq 0, \alpha^2 = 0$) is discussed in the text.

¹⁰⁰ K. Maki (private communication).

stitial-gas concentrations. The theoretical $h^*(t)$ curves all assume $\alpha=1.825$ ($\alpha^2=3.33$), close to the value calculated from the normal-state electronic parameters (Table II, No. 22a). The experimental $h^*(t)$ points for the present, the Cape, and the Barnes and Hake data utilize the respectively measured values

$$(-dH_u/dT)_{T_c} = 36, 33, 34.1 \text{ kG/}^\circ\text{K}$$

and

$$-(dH_u/dt)_{t=1} = T_c(-dH_u/dT)_{T_c} = 150, 135, 145 \text{ kG.}$$

The present upper-critical-field data as plotted in Figs. 13–15 show that the experimental $h^*(t)$ for Ti(16 at. % Mo) lies between the theoretical curves for $\lambda_{s0}=0$ and $\lambda_{s0}=\infty$, implying the influence of spin-flip scattering. A fair over-all fit of the present $H_u(T)$ or $h^*(t)$ data to the WHH theory is obtained for $\lambda_{s0}=0.5$ as shown in Fig. 13. Cape⁴² previously deduced $\lambda_{s0}\approx 0.7$

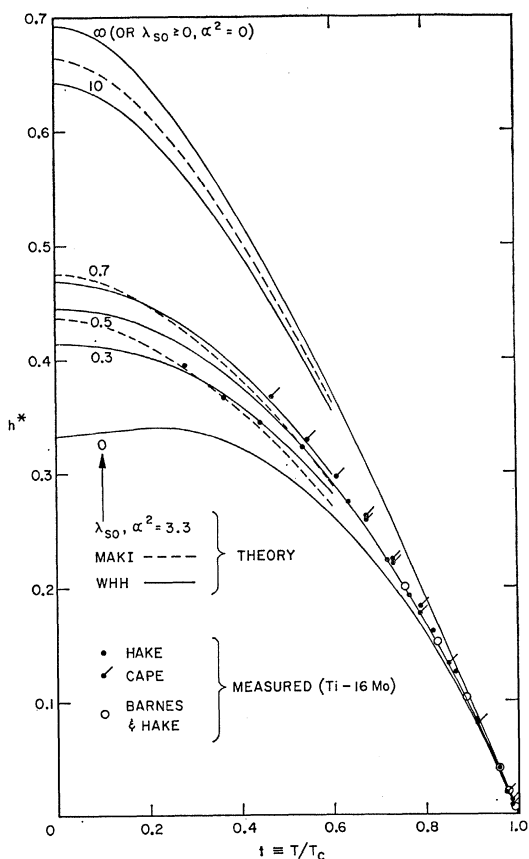


FIG. 14. Upper critical field $h^*(t) \equiv H_u(t)/(-dH_u/dt)_{t=1}$ versus reduced temperature t from the present magnetization measurements on Ti(16 at. % Mo) No. 1 (Fig. 4), the magnetization measurements of Cape (Ref. 42), and the calorimetric measurements of Barnes and Hake (Ref. 45). The theoretical Maki $h^*(t, \alpha, \lambda_{s0})$ curves are obtained from Eqs. (25) and (26) of the text and the WHH $h^*(t, \alpha, \lambda_{s0})$ curves are obtained by computer solution of Eq. (28) of Ref. 29. The maximum in the WHH curve $h^*(t, \alpha^2=3.3, \lambda_{s0}=0)$ signifies the onset, as t is reduced, of a first-order upper-critical-field transition to the normal state. In the region where dh^*/dt is positive, $h^*(t)$ is a supercooling field.

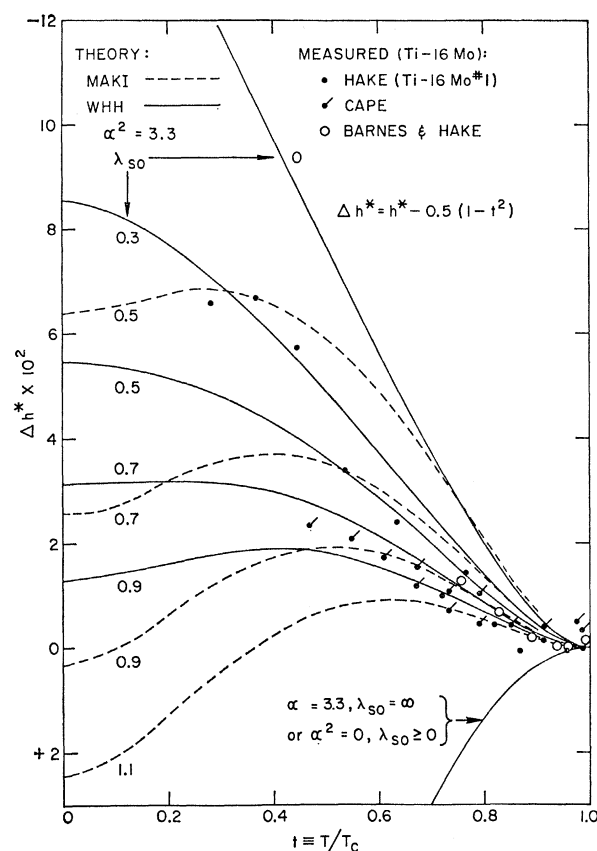


FIG. 15. Differential reduced upper critical field $\Delta h^* \equiv h^* - 0.5(1-t^2)$ versus reduced temperature t for the present magnetization measurements on Ti(16 at. % Mo) No. 1, the magnetization measurements of Cape (Ref. 42), and the calorimetric measurements of Barnes and Hake (Ref. 45). The theoretical Maki $\Delta h^*(t, \alpha, \lambda_{s0})$ is obtained from Eqs. (25) and (26) of the text and the WHH $\Delta h^*(t, \alpha, \lambda_{s0})$ is obtained via computer solution of Eq. (28) of Ref. 29.

for Ti(16 at. % Mo). The presently indicated λ_{s0} , τ_{80} , τ_{80}^{-1} , and τ_{tr}/τ_{80} values are listed in Table II, Nos. 29 to 31.

Figure 16 shows that κ_1^* for Ti(16 at. % Mo) No. 1, and for the other specimens of this study, decreases with decrease of t . For all these specimens $\kappa_1(t=1)$ is assumed to be equal to the Gor'kov-Goodman-calculated κ_G of Table II, No. 15c. For Ti(16 at. % Mo) No. 1, $H_c(t)$ is obtained from the calorimetric measurements⁴⁵ as discussed under Eq. (2). For the other specimens, $H_c(T)$ is calculated from the BCS⁹⁶ Eqs. (A12a) and (A12b). The theoretical Maki²⁸ $\kappa_1^*(\beta_0^2, t)$ curves of Fig. 16 are from Eqs. (10), (25), and (26), using the BCS deviation function $D_{BCS}(t)$. Replacement in Eq. (10) of $D_{BCS}(t)$ by the calorimetrically indicated⁴⁵ $D_{TM}(t)$ of Ti(16 at. % Mo) has little effect on the theoretical $\kappa_1^*(t < 0.6)$, but lowers the theoretical $\kappa_1^*(t \approx 0.9)$ about 6%. For clarity, and to avoid some redundancy (since we are also plotting h^*), the WHH curves for $\kappa_1^*(\alpha, \lambda_{s0}, t)$ via Eq. (10) are not shown in

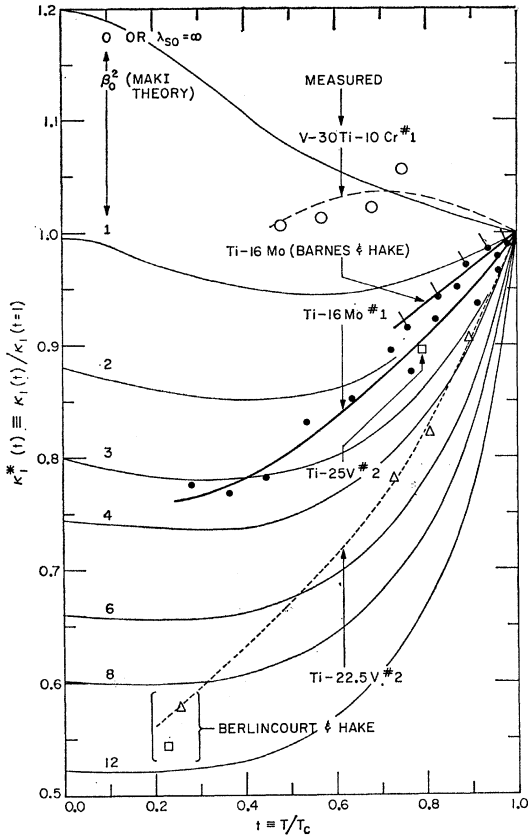


FIG. 16. The upper-critical-field parameter $\kappa_1^*(t) \equiv \kappa_1(t)/\kappa_1(t=1)$ versus reduced temperature t from present magnetization measurements, the calorimetric measurements of Barnes and Hake (Ref. 45), and the resistive-onset measurements of Berlincourt and Hake (Ref. 16). Except for the Ti(16 at. % Mo) data, all the data assume the BCS thermodynamic critical field of Eqs. (A12a) and (A12b). The theoretical curves of Maki (Ref. 28) are shown for various values of $\beta_0^2 \equiv \alpha^2/(1.78 \lambda_{s0})$ and are derived from Eqs. (10), (25), and (26) of the text assuming a BCS thermodynamic-critical-field deviation function.

Fig. 16. For comparison with magnetization data, Fig. 16 also shows the calorimetrically deduced⁴⁵ $\kappa_1^*(t)$ for Ti(16 at. % Mo).

b. *Terminal Mixed-State Magnetization Slope.* Figure 17 compares the present $\kappa_2^*(t)$ data for Ti(16 at. % Mo) No. 1 with the theoretical $\kappa_2^*(\beta_0^2, t)$ curves of Maki. Shown for comparison are the data of Cape,⁴² and the calorimetrically derived data of Barnes and Hake.⁴⁵ The present, the Cape, and the Barnes and Hake data assume respective values of $\kappa_2(t=1) = 68$ (κ_G , Table II, No. 15c), 65 [$\kappa_2(t \rightarrow 1)$ by extrapolation], and 61 [$\kappa_1(t=1)$ from Rutgers equation, $\Delta C(T_c)$, and $(dH_u/dT)_{T_c}$]. The present $\kappa_2^*(t)$ is in fair agreement with the Maki curve for $\beta_0^2 = 2$, implying, from Eq. (21) and the present $\alpha^2 = 3.3$, a $\lambda_{s0} = 0.93$, somewhat higher than the $\lambda_{s0} \approx 0.5$ derived above by means of a WHH fit to the $h^*(t)$ data.

2. V(30 at. % Ti) (10 at. % Cr), Ti(22.5 at. % V), and Ti(25 at. % V)

Because of the higher H_u and T_c values and the present experimental (H, T) limitations, the magnetization data for the other specimens of this study are much less complete than for Ti(16 at. % Mo) No. 1. Nevertheless, a tentative comparison of the present results with theory seems worthwhile. It is assumed, as for Ti(16 at. % Mo) No. 1, that $\kappa_1(t=1) = \kappa_2(t=1) = \kappa_G$, where κ_G is the Gor'kov-Goodman-calculated parameter of Table II, No. 15c. Figures 16 and 18 show, respectively, $\kappa_1^*(t)$ and $h^*(t)$ as derived from the magnetization-determined upper critical fields of V(30 at. % Ti) (10 at. % Cr) No. 1, Ti(22.5 at. % V) No. 2, and Ti(25 at. % V) No. 2. Also shown are two low- t points derived from the earlier resistive-onset measurements of Berlincourt and Hake.¹⁶ In Fig. 16, both the theoretical $\kappa_1^*(\beta_0^2, t)$ and the presently considered experimental $\kappa_1^*(t)$ points assume the BCS⁹⁶ $H_c(t)$ of Eqs. (A12a) and (A12b). The assumption of a BCS-type $H_c(t)$ for Ti-V alloys is supported by the calorimetric observation of Cheng *et al.*¹⁰¹ that for Ti-V (just as for Ti-Mo^{45,52}) the zero-field superconducting-state electronic specific heat $C_{es}(4 \gtrsim T_c/T \gtrsim 2)$ has a near BCS-like exponential temperature dependence. In Fig. 18, $h^*(t)$ is obtained from Eq. (6) in terms of the measured

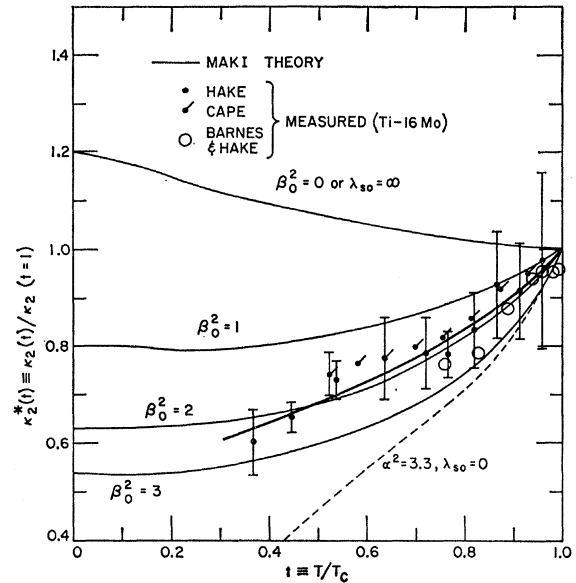


FIG. 17. The terminal mixed-state magnetization slope parameter $\kappa_2^*(t) \equiv \kappa_2(t)/\kappa_2(t=1)$ versus reduced temperature t from the present magnetization measurements on Ti(16 at. % Mo) No. 1, the magnetization measurements of Cape (Ref. 42), and the calorimetric measurements of Barnes and Hake (Ref. 45). The theoretical curves of Maki (Ref. 28) are shown for various values of $\beta_0^2 \equiv \alpha^2/(1.78 \lambda_{s0})$. The theoretical curve for $(\alpha^2 = 3.3, \lambda_{s0} = 0)$ is via an interpolation of curves given for the $\lambda_{s0} = 0$ case by Saint-James *et al.* (Ref. 31).

¹⁰¹ C. H. Cheng, K. P. Gupta, E. C. van Reuth, and P. A. Beck, Phys. Rev. **126**, 2030 (1962).

$H_u(t)$ and the calculated H_{c20}^* of Table II, No. 20a, since $(-dH_u/dt)_{t=1}$ was not measured. The λ_{s0} , τ_{s0} , τ_{s0}^{-1} , and τ_{tr}/τ_{s0} values suggested by a WHH-theory fit to the h^* data of Fig. 18 are listed in Table II, Nos. 29 to 31.

Figure 19 shows $\kappa_2^*(t)$ data for V(30 at.% Ti) (10 at.% Cr) No. 1, Ti(22.5 at.% V) No. 2, and Ti(25 at.% V) No. 2. The λ_{s0} , τ_{s0} , τ_{s0}^{-1} , and τ_{tr}/τ_{s0} values indicated by comparison of the data with the Maki $\kappa_2^*(\beta_0^2, t)$ curves are again listed in Table II, Nos. 29 to 31.

3. General Comparison

In general, Figs. 13-19 show extreme type-II high-field behavior which is consistent with the WHH and Maki theories, although complete quantitative accord is not obtained:

(a) The reduced parameters $h^*(t)$, $\kappa_1^*(t)$, and $\kappa_2^*(t)$ are always higher than theoretically expected

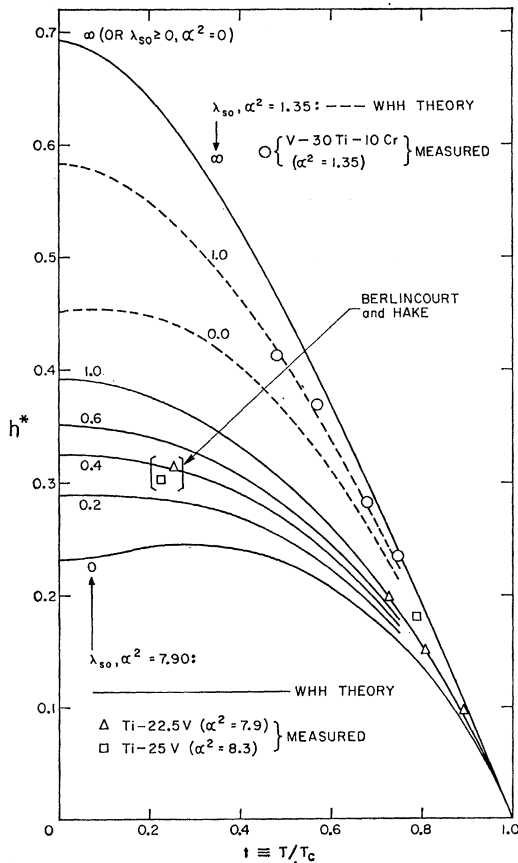


FIG. 18. Upper critical field $h^*(t) \equiv 0.693 H_u(t)/H_{c20}^*$ versus reduced temperature t from the present magnetization measurements on V(30 at.% Ti) (10 at.% Cr) No. 1, Ti(22.5 at.% V) No. 2, and Ti(25 at.% V) No. 2. Also shown are two points derived from the earlier resistive-onset measurements of Berlin-court and Hake (Ref. 16) on other specimens of Ti-V. The WHH theory $h^*(t, \alpha, \lambda_{s0})$ curves are obtained by computer solution of Eq. (28) of Ref. 29.

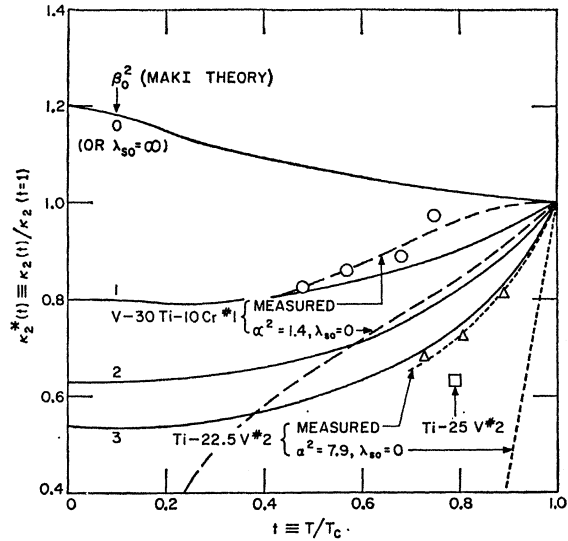


FIG. 19. The terminal mixed-state magnetization-slope parameter $\kappa_2^*(t) \equiv \kappa_2(t)/\kappa_2(t=1)$ versus reduced temperature t from the present magnetization measurements. The theoretical curves of Maki (Ref. 28) are shown for various values of $\beta_0^2 \equiv \alpha^2/(1.78 \lambda_{s0})$. The theoretical curve for $(\alpha^2=1.4, \lambda_{s0}=0)$ is via an interpolation of curves given for the $\lambda_{s0}=0$ case by Saint-James *et al.* (Ref. 31). The curve for $(\alpha^2=7.9, \lambda_{s0}=0)$ is from Maki's Eq. (27) of Ref. 28 for $t \approx 1$.

for the case $\lambda_{s0}=0$ but well below those theoretically expected for the case $\lambda_{s0} \rightarrow \infty$, implying a moderate influence of spin-flip scattering. On the basis of the WHH and Maki theories the data suggest λ_{s0} values in the range 0.5 to 1.3 (Table II, No. 29), and reasonable^{91,92} τ_{tr}/τ_{s0} ratios in the range 0.007 to 0.044 (Table II, No. 31), implying 0.7 to 4 spin flips for every 100 electronic collisions. Assuming that the WHH and Maki theories are essentially correct, the presently indicated nonzero λ_{s0} values are probably not merely the result of an overestimate of the appropriate $\alpha \equiv \sqrt{2}H_{c20}^*/H_{p0} = 2.35\rho_n\gamma$. In order to account for the experimentally suggested $h^*(t=0)$ values on the basis of the WHH theory with $\lambda_{s0}=0$ would require, from Fig. 12, $\alpha(\lambda_{s0}=0) = 1.3$ for Ti(16 at.% Mo) No. 1 [$h^*(t=0) \approx 0.42$], and $\alpha(\lambda_{s0}=0) = 1.8$ for Ti(22.5 at.% V) No. 2 [$h^*(t=0) \approx 0.33$]. These $\alpha(\lambda_{s0}=0)$ values are, respectively, 28% and 36% lower than the $\alpha = 2.35\rho_n\gamma = 1.81, 2.81$ calculated for Ti(16 at.% Mo) No. 1 and Ti(22.5 at.% V) No. 2, while ρ_n and γ values are probably accurate, respectively, to 3 and 5%. That appropriate α values have been used is also supported by the fact that the $\alpha = 1.91$ calculated for Ti(16 at.% Mo) No. 1 from the slope of the upper critical field curve near T_c via Eq. (A18c) is in fair agreement with the $\alpha = 2.35\rho_n\gamma = 1.81$ value (Table II, No. 22).

Since the present specimens all have relatively low average atomic number Z , one expects relatively low τ_{tr}/τ_{s0} ,^{37,92} The present narrow Z range (Table II, No. 8), and the approximate nature of the estimated

τ_{tr}/τ_{so} (Table II, No. 31), does not permit a meaningful test of the expected^{87,92} $\tau_{tr}/\tau_{so} \propto \langle Z^4 \rangle$.

(b) As predicted by the WHH and Maki theories, and as expected from the qualitative arguments of Sec. V.A, both κ_1 and κ_2 approach κ_G as $t \rightarrow 1$. This is shown in Figs. 16, 17, and 19, where, for the present magnetization data, $\kappa_i^*(t \rightarrow 1) = \kappa_i(t \rightarrow 1)/\kappa_G \approx 1$, and $i = 1, 2$.

(c) For each of the present specimens the ratio $\kappa_2^*(t)/\kappa_1^*(t) = \kappa_2(t)/\kappa_1(t) < 1$, consistent with Maki's²⁸ prediction that

$$1 \geq \kappa_2(t=0)/\kappa_1(t=0) \geq 0.29. \quad (27)$$

Linear extrapolation of the present Ti(16 at. % Mo) No. 1 data yields

$$\kappa_2(t=0)/\kappa_1(t=0) \approx 0.73. \quad (28)$$

The $\kappa_2(t)/\kappa_1(t)$ ratios for the present specimens at the lowest temperatures of measurement are listed in Table II, No. 34.

(d) The detailed t dependence of the upper-critical-field parameters h^* and κ_1^* does not appear to be in good agreement with the WHH and Maki theories; better agreement occurs for the terminal mixed-state magnetization slope parameter κ_2^* . Figures 13, 14, and 18 show a more pronounced flattening of $h^*(t)$ as $t \rightarrow 0$ than is predicted by the theories. Similar $h^*(t)$ curvature has been observed by others in resistive-onset measurements of dirty high- κ_G materials.^{29,33,34,36-38} Figure 16 shows the corresponding behavior of κ_1^* , i.e., a sharper fall in $\kappa_1^*(t)$ as $t \rightarrow 0$ than is theoretically predicted. Such h^* and κ_1^* curvature could be interpreted as indicating that the effective λ_{so} decreases as $t \rightarrow 0$.

Another disparity between theory and experiment is that in general somewhat different values for λ_{so} are indicated by $h^*(t)$ and $\kappa_2^*(t)$ data on the same specimen as shown in Table II, No. 29. This same feature was also observed for Ti(16 at. % Mo) by Cape.⁴² Computer solutions of Maki's more exact $\kappa_2(t)$ expression, Eq. (43) of Ref. 28, would be of interest in this regard.

(e) First-order transitions to the normal state are not observed down to the lowest temperatures of measurement, in agreement with the theories. According to Maki,²⁸ first-order transitions should be observed for the case $\lambda_{so} = 0$ if $\alpha > 1$. The reduced temperature t_f below which such first-order transitions should occur increases with α , i.e., $t_f(\alpha \geq 1, \lambda_{so} = 0) \geq 0$, and is indicated in Figs. 14 and 18 by the positions of the maxima in the theoretical $h^*(\lambda_{so} = 0)$ curves. Below these maxima, h^* is the supercooling field. Unfortunately, the present magnetization measurements do not extend to the interesting range $t < t_f$. However, the $\kappa_2^*(t)$ data of Figs. 17 and 19 do not suggest the first-order-transition condition $\kappa_2^* \rightarrow 0$ as $t \rightarrow 0$. According to the WHH theory,²⁹ first-order transitions should not occur for $\lambda_{so} > 0.5$, even for $\alpha \rightarrow \infty$. Closely related to this spin-orbit suppression of extreme type-II first-order transitions to the normal state is the possible spin-orbit

suppression of the Fulde-Ferrell state⁸⁷⁻⁸⁹ (although this state may not occur in a dirty superconductor even for $\lambda_{so} = 0$ ^{26,88,89}), and spin-orbit suppression of the tendency of localized magnetic moments to lower the superconducting transition temperature.^{91,102,103}

VI. CONCLUSIONS

The present results show that extremely "dirty," high- α , transition-metal-alloy superconductors with sufficiently low extended-defect concentrations display a new type of superconducting behavior characterized by reversible *paramagnetic* superconductivity.

The observed second-order upper-critical-field transitions between the paramagnetic mixed state and the paramagnetic normal state in these extremely dirty superconductors indicates the presence of considerable mixed-state Pauli paramagnetism near the upper critical field H_u . Comparison of the present $H_u(T)$, $\kappa_1(T)$, and $\kappa_2(T)$ data with the extreme-type-II WHH and Maki theories^{28,29} suggests that mixed-state paramagnetism is enhanced by spin-orbit-coupling-induced electronic spin-flip scattering, which acts to decouple superconductive Cooper spin-pairing, as first suggested by Ferrell⁹⁰ and Anderson.⁹¹ However, the present data do not appear to corroborate the finer details of the H_u and κ_1 temperature dependences as given by the theories.^{28,29}

Further magnetization studies on quasireversible high- κ_G superconductors as a function of reduced temperature t , dirtiness parameter ξ_0/l , paramagnetic limitation parameter α , average atomic number \bar{Z} ,³⁷ and localized-magnetic-moment concentration would be of value. Particularly deserving of early experimental investigation are (1) the low-reduced-temperature predictions of the Maki and WHH theories with regard to the curvature of $h^*(t)$ and the onset of first-order transitions at low λ_{so} , (2) the high-field magnetization behavior of "clean," low λ_{so} , quasireversible, high- κ_G materials,^{87,88,104} and (3) the extent to which the paramagnetic limitation on upper critical fields can be removed by controlled enhancement of spin-flip scattering.³⁷

ACKNOWLEDGMENTS

We wish to thank D. M. Sellman for able assistance with the apparatus and measurements; H. Nadler, R. G. Herron, R. E. Rayburn, and J. W. Savage for careful specimen preparation; C. G. Rhodes, D. G. Swarthout, and R. A. Spurling for optical, electron, and x-ray metallography; F. E. Knuth for expert machining of solenoid forms; N. R. Werthammer, E. Helfand, and P. C. Hohenberg for use of their computer pro-

¹⁰² L. P. Gor'kov and A. I. Rusinov, Zh. Eksperim. i Teor. Fiz. **46**, 1363 (1964) [English transl.: Soviet Phys.—JETP **19**, 922 (1964)].

¹⁰³ K. H. Bennemann, Phys. Rev. Letters **17**, 438 (1966).

¹⁰⁴ C. G. Shull and F. A. Wedgwood, Phys. Rev. Letters **16**, 513 (1966).

gram for the solution of $h^*(\alpha, \lambda_{80}, t)$; S. T. Imrich for computer-processing advice; and T. G. Berlincourt for valuable discussions.

APPENDIX

The formulas used to calculate or estimate the electronic properties of Table II are listed below in terms of experimentally convenient parameters and units: the low-temperature normal-state electrical resistivity ρ_n (Ω cm), the normal-state electronic-specific-heat coefficient γ ($\text{erg cm}^{-3}\text{K}^{-2}$), the superconducting transition temperature T_c ($^\circ\text{K}$), the conduction electron density n (cm^{-3}), and the ratio S/S_f of the free Fermi surface area S to that of a free-electron gas of density n . Other symbols and units are the free Fermi surface in wave-vector space S_k (cm^{-2}), the BCS half-energy gap at zero temperature Δ_{00} (erg), the Bohr magneton μ_B (erg G^{-1}), Planck's constant h or $\hbar = h/2\pi$ (erg sec), Boltzmann's constant k_B ($\text{erg }^\circ\text{K}^{-1}$), the electron charge e (esu), and the velocity of light c (cm sec^{-1}).

1. Average Fermi velocity¹⁰⁵:

$$\begin{aligned} \langle V_F \rangle &\geq \langle 1/V \rangle_F^{-1} = k_B^2 S_k (6h\gamma)^{-1} \\ &= 5.76 \times 10^{-5} n^{2/3} (S/S_f) \gamma^{-1} \text{ cm/sec,} \end{aligned} \quad (\text{A1})$$

where the equality holds for a spherical Fermi surface.

2. Electron mean free path¹⁰⁵:

$$\begin{aligned} l &= 6\pi^2 \hbar [e^2 S_k \rho_n]^{-1} \\ &= 1.27 \times 10^4 [\rho_n n^{2/3} (S/S_f)]^{-1} \text{ cm,} \end{aligned} \quad (\text{A2})$$

where the first ρ_n is in esu and the second ρ_n is in Ω cm.

3. Thermal effective electron-mass ratio:

$$(m^*/m)_t \equiv \gamma/\gamma \text{ (free electron)} = 6.21 \times 10^4 \gamma n^{-1/3}. \quad (\text{A3})$$

4. Transport scattering time:

$$\tau_{tr} \approx l \langle 1/V \rangle_F = 2.21 \times 10^8 \gamma [\rho_n n^{4/3} (S/S_f)^2]^{-1} \text{ sec,} \quad (\text{A4})$$

using Eqs. (A1) and (A2).

5. Density of states of one spin direction:

$$\begin{aligned} N &= \gamma (\frac{2}{3}\pi^2 k_B^2)^{-1} = 8.0 \times 10^{30} \gamma \text{ erg}^{-1} \text{ cm}^{-3} \\ &= 0.212 \gamma \text{ eV}^{-1} \text{ atom}^{-1}, \end{aligned} \quad (\text{A5})$$

where the last γ only is in units of $[mJ \text{ mole}^{-1} (^\circ\text{K})^{-2}]$ and mole means Avogadro's number of atoms.

6. Pauli spin susceptibility:

$$\begin{aligned} \chi_P(N) &= 2\mu_B^2 N = 3\mu_B^2 \gamma (\pi^2 k_B^2)^{-1} \\ &= 1.37 \times 10^{-9} \gamma \text{ emu cm}^{-3}. \end{aligned} \quad (\text{A6})$$

¹⁰⁵ See, for example, A. B. Pippard, *Reports on Progress in Physics*, (Institute of Physics and the Physical Society, London, 1960), Vol. XXIII, p. 176.

7. BCS coherence length⁹⁶:

$$\begin{aligned} \xi_0 &= \hbar \langle V_F \rangle (\pi \Delta_{00})^{-1} = 0.180 \hbar \langle V_F \rangle (k_B T_c)^{-1} \\ &\approx 7.93 \times 10^{-17} n^{2/3} (S/S_f) (\gamma T_c)^{-1} \text{ cm,} \end{aligned} \quad (\text{A7})$$

using Eq. (A1) and assuming $\langle V_F \rangle \approx \langle 1/V \rangle_F^{-1}$.

8. Ginzburg-Landau coherence length ($\xi_0 \gg l$)^{106,107}:

$$\begin{aligned} \xi_G &\approx (\xi_0 l)^{1/2} (1-t)^{-1/2} \\ &\approx 1.0 \times 10^{-6} (\rho_n \gamma T_c)^{-1/2} (1-t)^{-1/2} \text{ cm,} \end{aligned} \quad (\text{A8})$$

using Eqs. (A2) and (A7), with $t \equiv T/T_c$.

9. Electromagnetic coherence length (0°K)^{106,108}:

$$\begin{aligned} \xi_e &\approx (\xi_0^{-1} + l^{-1})^{-1} \\ &= \{ 1.26 \times 10^{16} \gamma T_c [n^{2/3} (S/S_f)]^{-1} \\ &\quad + 7.87 \times 10^{-5} \rho_n n^{2/3} (S/S_f) \}^{-1} \text{ cm,} \end{aligned} \quad (\text{A9})$$

using Eqs. (A2) and (A7).

10. London penetration depth (0°K)^{16,109,110}:

$$\begin{aligned} \lambda_{L0} &= 3ch\gamma^{1/2} \pi^{1/2} (ek_B S_k)^{-1} \\ &= 1.33 \times 10^8 \gamma^{1/2} [n^{2/3} (S/S_f)]^{-1} \text{ cm.} \end{aligned} \quad (\text{A10})$$

11. Penetration depth (0°K , $\lambda \gg l$, $\xi_0 \gg l$)^{106,108}:

$$\lambda_0 \approx \lambda_{L0} (\xi_0/l)^{1/2} = 1.05 \times 10^{-2} (\rho_n/T_c)^{1/2} \text{ cm,} \quad (\text{A11})$$

using Eqs. (A2), (A7), and (A10).

12. Thermodynamic critical field (BCS)⁹⁶:

$$\text{a. } H_c = H_{c0} (1-t^2) + D_{\text{BCS}}(t) H_{e0}, \quad (\text{A12a})$$

$$\text{b. } H_{e0} = 2.42 \gamma^{1/2} T_c G, \quad (\text{A12b})$$

where $D_{\text{BCS}}(t) \equiv$ BCS deviation function¹¹¹.

13. Gor'kov-Goodman-calculated Ginzburg-Landau parameter $\kappa_G^{1,3,16,20,22,112}$:

- a. intrinsic:

$$\kappa_o = 0.96 \lambda_{L0} \xi_0^{-1} = 1.61 \times 10^{24} \gamma^{3/2} T_c [n^{4/3} (S/S_f)^2]^{-1}, \quad (\text{A13a})$$

using Eqs. (A7) and (A10);

- b. extrinsic:

$$\kappa_t = ec\gamma^{1/2} \rho_n (k_B \pi^3)^{-1} [21\zeta(3)/2\pi]^{1/2} = 7500 \rho_n \gamma^{1/2}, \quad (\text{A13b})$$

where $\zeta(3) = 1.202$;

- c. total:

$$\kappa_G = \kappa_o + \kappa_t, \quad (\text{A13c})$$

to within 6% for all $\xi_0 l^{-1}$ and to within 2.5% for the present $\xi_0 l^{-1} > 38$ ⁸.

¹⁰⁶ P. G. de Gennes, *Superconductivity of Metals and Alloys*, translated by P. A. Pincus (W. A. Benjamin, Inc., New York, 1966), pp. 24, 225.

¹⁰⁷ C. Caroli, P. G. de Gennes, and J. Matricon, *Physik Kondensierten Materie* **1**, 176 (1963); C. Caroli, *ibid.* **3**, 345 (1965).

¹⁰⁸ A. B. Pippard, *Proc. Cambridge Phil. Soc.* **47**, 617 (1951); *Proc. Roy. Soc. (London)* **A216**, 547 (1953).

¹⁰⁹ B. B. Goodman, *Phys. Letters* **1**, 215 (1962).

¹¹⁰ T. E. Faber and A. B. Pippard, *Proc. Roy. Soc. (London)* **A231**, 336 (1955).

¹¹¹ See, for example, J. C. Swihart, *IBM J. Res. Develop.* **6**, 14 (1962).

¹¹² B. B. Goodman, *IBM J. Res. Develop.* **6**, 63 (1962).

14. Ginzburg-Landau parameter $\kappa_1(T_c)$:

$$\begin{aligned}\kappa_1(T_c) &= (dH_u/dT)_{T_c} / [\sqrt{2}(dH_c/dT)_{T_c}] \\ &= (6.0\gamma^{1/2})^{-1} (-dH_u/dT)_{T_c},\end{aligned}\quad (\text{A14})$$

assuming, from BCS,⁹⁷ $(dH_c/dT)^2_{T_c} = 18.0\gamma$.

15. Lower critical field ($\xi_0 \gg l$)²⁷:

$$H_{c1}(t) = \sqrt{2}H_c(t) \{ [ln\kappa_3(t)] / [2\kappa_3(t)] \} \quad (\text{A15})$$

where $\kappa_3(t) = \kappa_3^*(t)\kappa_G$, $\kappa_3^*(t) \equiv \kappa_3(t)/\kappa_3(t=1)$ is given graphically by Maki, $\kappa_3^*(t=0) = 1.53$, and κ_G is given by Eq. (A13c).

16. Neo-GLAG⁹⁻¹⁴ nonparamagnetically limited upper critical field ($\xi_0 \gg l$, 0°K):

$$\text{a. } H_{c20}^* = \sqrt{2}[\kappa_1(0^\circ\text{K})/\kappa_1(T_c)]\kappa_1(T_c)H_{c0}; \quad (\text{A16a})$$

$$\text{b. } H_{c20}^* \approx 3.06 \times 10^4 \rho_n \gamma T_c G, \quad (\text{A16b})$$

by substitution of¹² $\kappa_1(0^\circ\text{K})/\kappa_1(T_c) = 1.195$, $\kappa_1(T_c) \approx \kappa_l = 7500\rho_n\gamma^{1/2}$, and $H_{c0}(\text{BCS}) = 2.42\gamma^{1/2}T_c$ in Eq. (A16a)].

c. From upper critical field slope^{28,29} [see Eq. (5)],

$$H_{c20}^* = 0.693T_c(-dH_u/dT)_{T_c}. \quad (\text{A16c})$$

17. Clogston upper-critical-field limit (0°K)²³:

$$\frac{1}{2}\chi_P H_{p0}^2 = H_{c0}^2/8\pi = \frac{1}{2}N\Delta_{00}^2; \quad (\text{A17a})$$

$$H_{p0} = \Delta_{00}(\sqrt{2}\mu_B)^{-1} = 1.84 \times 10^4 T_c G, \quad (\text{A17b})$$

substituting $\chi_P = 2\mu_B^2 N$ of Eq. (A6) into Eq. (A17a).

18. Maki paramagnetic limitation parameter²⁸:

$$\text{a. } \alpha \equiv \sqrt{2}H_{c20}^*/H_{p0}; \quad (\text{A18a})$$

$$\text{b. } \alpha = 2.35\rho_n\gamma, \quad (\text{A18b})$$

substituting Eqs. (A16b) and (A17b) into Eq. (A18a), $\xi_0 \gg l$ is assumed;

$$\text{c. } \alpha = 5.33 \times 10^{-5} (-dH_u/dT)_{T_c}, \quad (\text{A18c})$$

substituting Eqs. (A16c) and (A17b) into Eq. (A18a).

19. Spin-flip scattering time²⁹:

$$\tau_{s0} = \hbar(3\pi k_B T_c \lambda_{s0})^{-1} = 8.11 \times 10^{-13} (T_c \lambda_{s0})^{-1} \text{ sec.} \quad (\text{A19})$$

Law of Corresponding States for fcc and d-hcp La*

D. L. JOHNSON AND D. K. FINNEMORE

Institute for Atomic Research and Department of Physics, Iowa State University, Ames, Iowa

(Received 19 December 1966)

The specific heats of fcc and d-hcp La have been measured from 1.0–10.0°K. There is a striking similarity between these two metals, and a law of corresponding states is obeyed for both the superconducting- and normal-state specific heats. An energy-gap parameter determined from both the temperature-dependent electronic specific heat and from the free-energy difference is $3.7kT_c$, in good agreement with the BCS value. No evidence is found for an *f*-band contribution to the superconducting characteristics.

INTRODUCTION

FOR several years theorists have speculated that certain transition-metal superconductors might show substantial deviations from a law of corresponding states. In 1959, Suhl, Matthias, and Walker¹ proposed a two-band model which gives a rather complicated excitation spectrum. In special circumstances it leads to independent energy gaps for each band. Indeed, there is preliminary evidence that Nb may exhibit this two-gap behavior.² In further theoretical work, Kondo³ has shown that exchange coupling between bands enhances superconductivity and he has proposed that this mechanism may be important in determining the relatively high transition temperature T_c of compounds like $V_3\text{Ga}$ and the element La. An alternate model

which is especially applicable for La has been proposed by Kuper, Jensen, and Hamilton.⁴ Here it is assumed that there is a narrow *f* band above, but very close to, the Fermi surface and that the coupling comes through an antiferromagnetic exchange. With reasonable approximations for the position of the *f* band and the strength of the coupling, the theory gives two energy gaps and strong deviations from a law of corresponding states.

The specific-heat measurements which are reported here were undertaken to look for evidence of this proposed *f* band near the Fermi surface and to look for deviations from a law of corresponding state. Since La occurs in two crystallographic modifications, there are essentially two different metals available for this work and the effects of crystal structure have been studied. Normal-state results have been analyzed in terms of deviations from the Sommerfeld and Debye⁵ theories

* Work performed in the Ames Laboratory of the U.S. Atomic Energy Commission. Contribution No. 2003.

¹ H. Suhl, B. T. Matthias, and L. R. Walker, Phys. Rev. Letters **3**, 552 (1959).

² L. Shen, N. M. Senozan, and N. E. Phillips, Phys. Rev. Letters **14**, 1025 (1965).

³ J. Kondo, Progr. Theoret. Phys. (Kyoto) **29**, 1 (1963).

⁴ C. G. Kuper, M. A. Jensen, and D. C. Hamilton, Phys. Rev. **134**, A15 (1964).

⁵ C. Kittel, *Introduction to Solid State Physics* (John Wiley & Sons, Inc., New York, 1966), 3rd ed.

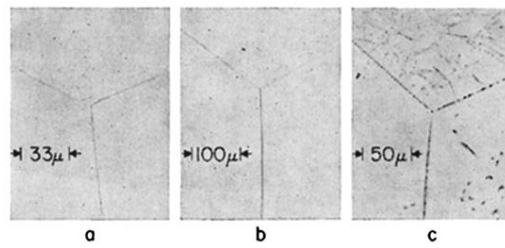


FIG. 1. Photomicrographs representative of (a) Ti(16 at.% Mo) No. 1 (annealed), (b) Ti(25 at.% V) No. 1 (as arc cast), and (c) Ti(25 at.% V) No. 3 (annealed), as discussed in the text and indicated in Table I.